Soil Dynamics and Earthquake Engineering 123 (2019) 470–497

Contents lists available at ScienceDirect

Soil Dynamics and Earthquake Engineering

journal homepage: www.elsevier.com/locate/soildyn

Site specific analysis using topography conditioned response spectra

Mario Sáenz, César Sierra*, Juan Vergara, Juan Jaramillo, Juan Gomez

Escuela de Ingeniería, Universidad EAFIT, Medellín, Colombia

ARTICLE INFO

Keywords:
Earthquake engineering
Topographic effects
Ground response analysis
Site effects

ABSTRACT

We address topographic effects in site response analysis. By splitting a generalized surface topography into simple geometric elements we identify fundamental concepts that control the dynamic response. We show that in the construction of a model for a particular topographic scenario the geometric details that must mandatory be retained into the model depend upon the expected period range of interest in the response spectra. We refer to this limited spectra as a topography conditioned response spectra. To fully test the newly introduced idea, we conducted extensive parametric analysis of the previously identified fundamental elements and generate a proxy to relate a lower bound of the target structural period to the maximum dimensionless frequency required in the model. This dimensionless frequency indicates accurately what elements of the profile can be eliminated as these are irrelevant for the spectral response. The proposed analysis technique is further explained using as case of study the topographic scenario corresponding to the Aburrá Valley region in Medellín, Colombia. Our results show that with relatively simple models we can predict accurately the spectral response up to the prescribed target period.

1. Introduction

The determination of the local response at a site under the occurrence of an earthquake event is an important and crucial aspect of seismic engineering that impacts microzonation studies, the generation of input motions for analysis and design of earthquake resistant structures, and in general, the results of seismic risk assessment analysis. Despite the fact that the local response is a function of several coupled effects such as non-linear soil behavior, mechanical amplification by soil stratification and presence of complex surface (and sub-surface) topography [16,28], most of the seismic provisions throughout the world incorporate methods based upon one-dimensional wave propagation models that fully neglect geometrical effects. Previous theoretical works, as well as field observations, have shown that such simplified techniques are insufficient in the prediction of surface ground motions. Probably the most striking proofs of the inaccuracies in one-dimensional wave propagation analysis methods are the (>1.0 g) recorded accelerations during the 1994 Northridge and the 1971 San Fernando earthquakes [14,41]. This paper deals with topographic effects introduced by surface topography and specifically with the connection between geometric features and the associated response spectra.

Among the many factors controlling the ground response at a site, the mechanical effect has been the most thoroughly studied: mechanical amplification is included in seismic codes in terms of site coefficients computed on the basis of the shear wave propagation velocity of the last 30 m of the deposit and used to modify an input response spectra specified for a reference station [4,22]. Clearly, such a simplistic approach implicitly considers vertical incidence of the wave field and a one-dimensional propagation model in which the site is assumed to be conformed by a horizontally-infinite stack of layers. One-dimensional (1D) based methods have been further improved to account for well known nonlinear soil behavior through equivalent linear algorithms where the inelastic soil properties are considered in terms of modulus reduction and damping ratio curves [37,13,19,44]. Topographic effects in the engineering community have been addressed mainly through 3 different approaches namely: (i) studies conducted in terms of closed-form solutions for simplified geometries which are relevant as they shed light on the fundamental physical aspects of the problem [40,42,43,46,18]; (ii) parametric analysis of simplified topographies performed using numerical simulations [5,16,8,30,31]; and (iii) numerical determination of the response in particular scenarios [15,27,32,38,39,26,6]. Although the numerical approach based on high performance computing has gain popularity due to the proliferation of robust numerical algorithms [12,45,24] and the increase in computing power the application of large scale models is still limited as these models require field data that is rarely available at the practicing level.

By contrast with the mechanical problem, and despite the fact that

* Corresponding author.
E-mail address: csierraa@eafit.edu.co (C. Sierra).

https://doi.org/10.1016/j.soildyn.2019.03.004
Received 7 November 2018; Received in revised form 11 February 2019; Accepted 7 March 2019
Available online 20 May 2019

the effect of surface and sub-surface topography has been identified as an important cause of damage concentration in many earthquakes [30,7], there is a lack of unified approaches to explicitly include them on site response analysis. This can be evidenced from the few seismic provisions with implemented procedures aimed at addressing topographic aggravation [22,1,10]. As concluded from mostly theoretical works, the main signature of the geometric effect on the response is the spatial variability in the ground motions [2,36,34,35]. Interestingly, although this implies a frequency dependence of the response, the few available code-based approaches use constant amplification factors that depend solely in local geometric parameters at the site. This work is devoted to the analysis of topographic effects through simplified and rationally built models intended to capture the incidence of surface geometry on the response at a site. We address the question of whether results based upon simplified models, built with limited field data, are of any use for engineering purposes. Although as demonstrated by other authors, the mechanical and geometric effects might become strongly coupled [6], here we focus on the influence of surface topography on the ground response. We follow an approach based on previous findings from geometric theory of diffraction and parametric analysis. Our work is aimed at identifying (i) the frequency range at which one should expect modifications in the ground motions for a given surface topography; (ii) what are the relevant geometric features from a given topographic profile if one is interested in the response within a prescribed frequency band and (iii) what is the effectiveness of simplified models to capture topographic effects.

Here these fundamental problems are studied with a hierarchical and rational analysis of a generalized topographic profile resulting after one splits the problem into simpler ones. To that end we start from the fact that a topographic profile can be represented through the combination of several adjacent concave and convex shapes of various characteristic dimensions. These dimensions define the topographic resolution and thus the expected frequency content of the response. This concept of topographic resolution is translated into a range of structural periods in the response spectra at which ground motion variation due to topographic effects should be expected. Since the characteristic dimension of the topographic relief is a conceptual physical parameter, it is not possible to modify its value during the analysis stage. However, one can use this idea to decide what geometrical features of the topographic relief are truly relevant for the prescribed range of target structural periods. In this research we establish a physical connection between surface topography and site effects in terms of response spectra. This connection is then used in the analysis of two cross sections of the Aburr Valley Region (AVR) in Medellín, Colombia. For each cross section we proposed 4 models with decreasing levels of complexity generating response spectra with limited range of validity. The region is a long-shaped sedimentary valley located in the northwestern corner of South America and it accommodates the city of Medellín, the second largest in Colombia, with an estimated population of 2.5 million people. The valley constitutes an interesting scenario to study site effects as there has been an increase in urban developments along the flanks of the mountainous system surrounding the city.

The current research will contribute to the understanding of topographic effects as it offers an alternative perspective involving the idea of simplified models based upon a target period range. Such conceptual development can also be used in a first order estimation of the expected frequency content of ground motions generated at a particular scenario. In the first part of the paper we focus on the response of a single wedge as suggested in the superposition based diffraction (SBD) method [21,17]. In order to obtain a systematic method of approximation to the model, we also study the response of an equivalent wedge resulting from a continuous curve tangent to the singular wedge. The smooth wedge introduces as geometric parameter the distance between both geometries: we refer to this parameter as the geometrical resolution d. The study of independent fundamental wedges, and specifically, its approximation by its smooth equivalents, is used in the next section to analyze two simplified topographies corresponding to trapezoidal canyons and hills. Thus, each topography is represented in terms of a singular and a smooth wedge. The canonical forms introduce a second geometric parameter corresponding to the distance between adjacent wedges L_W. An error estimate is then introduced as the normalized difference between the amplitude of the transfer function for the singular and the smoothed wedge. These analysis allows us to obtain dimensionless frequency ranges for which the error estimate remains below a prescribed value indicating that the response from the singular and the smooth wedge approximation are equivalent. That result is later used to derive a recipe for the geometric resolution as a function of a target frequency. The main result from this section is a systematic criteria to eliminate (or introduce into the model) topographic features whose characteristic dimension varies within a band of size $2d$. The resulting band method is then applied to a realistic topography, corresponding to the AVR-region in Medellin, Colombia. The paper ends with conclusions and a proposal for further work.

2. Effective response of a topographic profile

To develop our method of analysis we introduce the concept of topographic element as the fundamental building block in terms of which the analyst can build an arbitrary topographic profile. Following the same approach in which one uses the maximum frequency of the incident field to define the appropriate element size in a numerical simulation of a wave propagation problem, here we use a target analysis frequency to select the appropriate level of topographic resolution. We postulate that in the calculation of ground motions the analyst prescribes a desired target level of accuracy for the spectral response implicitly prescribing the topographic elements that are required to reach that accuracy. The target frequency is related to the range of structural periods for which the site effects analysis is conducted in the first place. As a consequence, the final model would include only that particular topographic information that is required for that specific analysis resulting in a simplified model. To study the impact in the response of the different levels of simplification we use the level of topographic resolution (associated to the size of the topographic element). This concept appears naturally following the contribution from Jaramillo et al. [21] where it is recognized that the main controlling factor of the spatial variation of the ground motion corresponds to geometric singularities existing in the topographic profile. Here we analyze models with different resolution levels using an approach based on the response of a simple semi-infinite wedge and leading to a systematic way of approximating a given topography.

2.1. Topographic resolution

We formalize the concept of topographic resolution as the frequency range of the wave field that can be effectively propagated by a physical topographic scenario. This is done after properly identifying a topographic element of characteristic dimension h_{top}. Such element is defined as the fundamental building block in terms of which it is possible to construct (or represent) a surface irregularity of arbitrary shape. Its characteristic dimension can be connected to the minimum wavelength of the incident field $\lambda^{\min}$ by the dimensionless frequency

$$\eta = \frac{h_{top}}{\lambda^{\min}}. \tag{1}$$

Notice that Eq. (1) is analogous to the relation between the minimum wavelength $\lambda^{\min}$, and the characteristic discretization size h_{num}, existing in a computational model intended for wave propagation analysis, in which case the dimensionless frequency parameter

$$\alpha = \frac{h_{num}}{\lambda^{\min}} \tag{2}$$

is indicative of the number of required elements per minimum

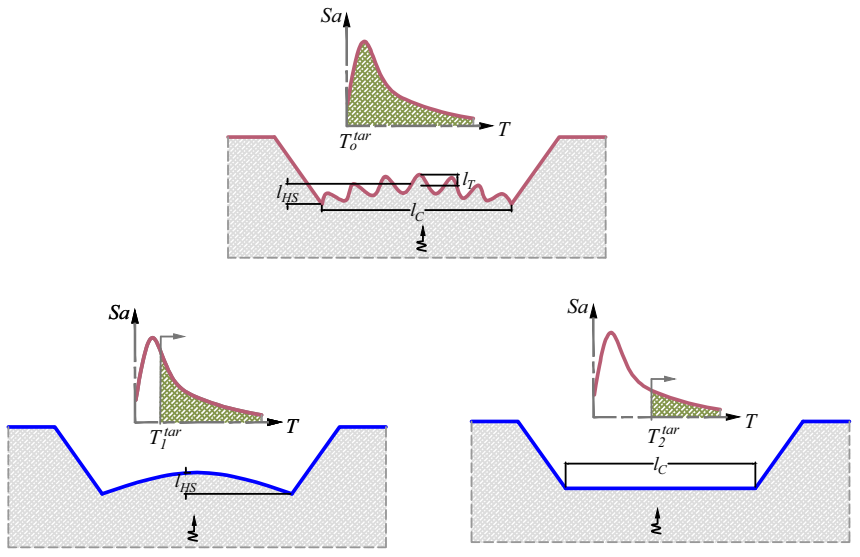

Fig. 1. Schematic description of topography-dependent-response-spectra (*TRS*). The figure represents a topographic scenario with geometric features of increasing characteristic dimension. The top part corresponding to the original unmodified profile includes 3 distinguishable geometric features: (i) a tooth-like topographic undulation of size ℓ_T at the bottom of the canyon; (ii) a half-sine hill of amplitude ℓ_{HS} also embedded in the bottom surface and (iii) the overall trapezoidal-shaped canyon of width ℓ_C. The target structural period T^{tar} sets the size h_{top}^{min} of the minimum topographic element that must be retained in each case in order to predict results accurate in the shaded period range.

wavelength. In wave propagation analysis conducted with the finite element method a commonly employed criteria corresponds to $\alpha = 0.1$ (or 10 elements per wavelength) [11,20]. Note also that, although in the current context of topographic effects η plays the same role as α in Eq. (2), here the dimensionless frequency parameter prescribes the number of wavelengths that fit into the topographic element, consequently the value of η specifies the quality or topographic resolution of the model. By contrast with the numerical problem, where one can always refine the discretization and enhance the model capabilities, in the topographic scenario h_{top} is rather a physical parameter that cannot be modified. However, as it will be shown later, once h_{top} is identified in a particular case, it can be used either to conduct first order estimates of the expected frequency content of the ground motions, or to decide what topographic features of the actual profile are effectively relevant for an input excitation of a given frequency content. It is now evident that in a realistic scenario the expected characteristics of the ground motions are a function of the topographic resolution prevailing in the surface geometry.

2.2. Topography-limited-response-spectra

The characterization of the topographic elements existing in a particular scenario, and specifically the concept of topographic resolution, can be used as an objective tool to identify the geometric features in a surface profile that are relevant if one is interested in predicting the response up to a target period. Thus, if one constructs a simplified model of the topographic profile where all the irrelevant geometric features are removed, introducing a limited resolution, then the resulting response spectra is accurate up to this target period: we refer to this specific response spectra as a topography-limited-response-spectra (*TRS*). To establish a connection between the target period and the relevant topographic elements we rewrite Eq. (1) as:

$$h_{top}^{min} = \eta \lambda^{tar} \tag{3}$$

and in which h_{top}^{min} specifies that all topographic irregularities of characteristic dimension $\ell < h_{top}^{min}$ are unnecessary if the analysis is intended to predict a *TRS* with accurate results up to $f^{tar} = \beta/\lambda^{tar}$, where β is the shear wave propagation velocity. Although the resulting simplified model may or may not lead to considerable computational savings, its most appealing aspect lies in the physical connection existing between the topographic features and the response spectra. To fix ideas, the concept of prescribed topographic resolution and its connection to a target structural period is illustrated in Fig. 1 where we schematize a surface profile with topographic irregularities of characteristic dimensions of various sizes together with its resulting *TRS*. In each case the shaded area in the response spectra represents the range of accurate results according to the given topographic resolution. The top scheme represents the original topographic scenario with a complete response spectra. Note that the original profile contains 3 different length scales corresponding to: (i) the width of the trapezoidal canyon ℓ_C; (ii) the amplitude ℓ_{HS} of the half-sine topographic feature and (iii) the smaller tooth-like undulation ℓ_T at the bottom of the canyon. Note also that $\ell_C > \ell_{HS} > \ell_T$. The bottom part of the figure describes two possible simplified models. The model on the left is the result of removing the smaller tooth-like feature at the bottom of the canyon yielding a response spectra valid for periods larger than T_1^{Tar}. Similarly, the model in the right results after removing the gentle half-sine hill at the bottom leaving only the symmetric trapezoidal canyon and a response spectra valid for periods larger than T_2^{Tar}. As suggested by this schematic description, the topographic resolution in a model of a surface profile can be decreased after removing elements at the expense of loosing high frequency content in the resulting response spectra. In the following section we define the topographic element and identify its characteristic dimension in such a way that we can proceed systematically in the identification of the expected frequency content associated to a given profile or, alternatively, in the modification of the profile to match a *TRS* as defined by a target period.

2.3. Fundamental topographic element

The infinite wedge has long been recognized as the fundamental building element present in complex topographic profiles. In the context of wave propagation analysis for seismic ground motions, pioneering work on the dynamic response of infinite (and finite) wedges can be found in contributions from Sánchez-Sesma [34,35]. More recently, the wedge as fundamental block was used by Mohammadi [29] and Asimaki and Mohammadi [6] in a parametric analysis of geometric and stratigraphic effects. These and other related works have identified the wedge as the fundamental topographic element or basic shape for the construction of very general topographic profiles. A seminal and landmark contribution to the subject was given by Keller [23] who provided the solution for the diffracted field resulting from the interaction between an incident wave and the corner singularity at the tip of the wedge in the context of electromagnetic waves. That work was elegantly cast into a geometric method, commonly known as geometric theory of diffraction (GTD), where the complete solution is built by the

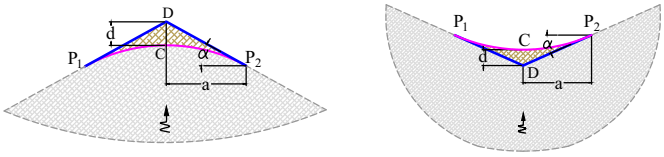

Fig. 2. Building block to be used in the approximate representation of topographical features of general shape. Each element is defined by the enclosing wedge with source of diffraction at D; its continuous curve C with contact points P_1 and P_2; and by the slope angle α. The actual surface may resemble the singular wedge (blue line) or the continuous tangent curve (magenta line). The separation distance d, which controls the differences in the response in each wedge, is a wavelength dependent function. However, up to a certain value of this resolution parameter both solutions are deemed equivalent implying that topographic features of dimension smaller than d are irrelevant for the required model.

superposition of incident, reflected and diffracted rays.

In a recent work Jaramillo et al. [21] and later Gomez et al. [17], used Keller's GTD theory to formulate a superposition method to build the solution for a surface profile subjected to incident *SH* waves. In that approach the topographic profile is represented by the superposition of several interconnected wedges while the total solution is found after adding fields produced by incident, reflected and diffracted rays. The diffracted rays result from the interaction of the wave field with the corner singularities from each wedge. The consideration of two or more adjacent wedges introduces interactions between contiguous topographic features corresponding to additional reflected and diffracted rays of the primary field generated by a single tip. In the final arrangement the interaction between topographic features is identified in the diffracted waves trapped within two singularities therefore becoming a function of the distance between wedges. Since, as shown by Keller [23] and Kouyoumjian and Pathak [25], the diffracted part of the solution decays with frequency the relevant parameter controlling this interaction ends up being the distance between wedges. In what follows we formalize the definition of this topographic element and propose an intrinsic characteristic dimension that can be used in Eq. (3) connecting the topographic element size to the target frequency from the response spectra. Two semi-infinite wedges, or in what follows topographic elements, describing a convex and a concave geometry are shown in Fig. ((2). Each element has as its defining geometric attributes the slope angle α and a corner singularity D: the singularity is a highly relevant component of the wedge since it is a source of diffracted waves in response to an incident wave. The infinite wedge does not have an intrinsic characteristic size as required by h_{top}^{min} in Eq. (3), however a characteristic dimension can be assigned if one leaves open the possibility to represent a topographic feature either by a singular or by a smooth surface. This idea is described in Fig. 2 in terms of a curve C, tangent to the wedge along points P_1 and P_2, and related to the singular wedge by the distance parameter d. According to Keller's GTD theory the smooth surface representation does not fully eliminate the diffracted field but instead, up to a given frequency range, the smooth surface is still perceived as a singular wedge. Since a given wedge admits an infinite set of tangent curves, for the dual smooth-singular wedge representation to remain valid, we must establish an equivalence criteria. In this work we will assume that the dual representation is valid for wedges whose distance parameter d is such that the dynamic response from both models yields results which are equal up to a prescribed normalized threshold. With diffraction being a wavelength dependent phenomena it turns out that for a given wedge the value of d is not unique but will depend on the frequency content of the incident field. Therefore this relationship can be written in terms of the target frequency introduced in (3) as

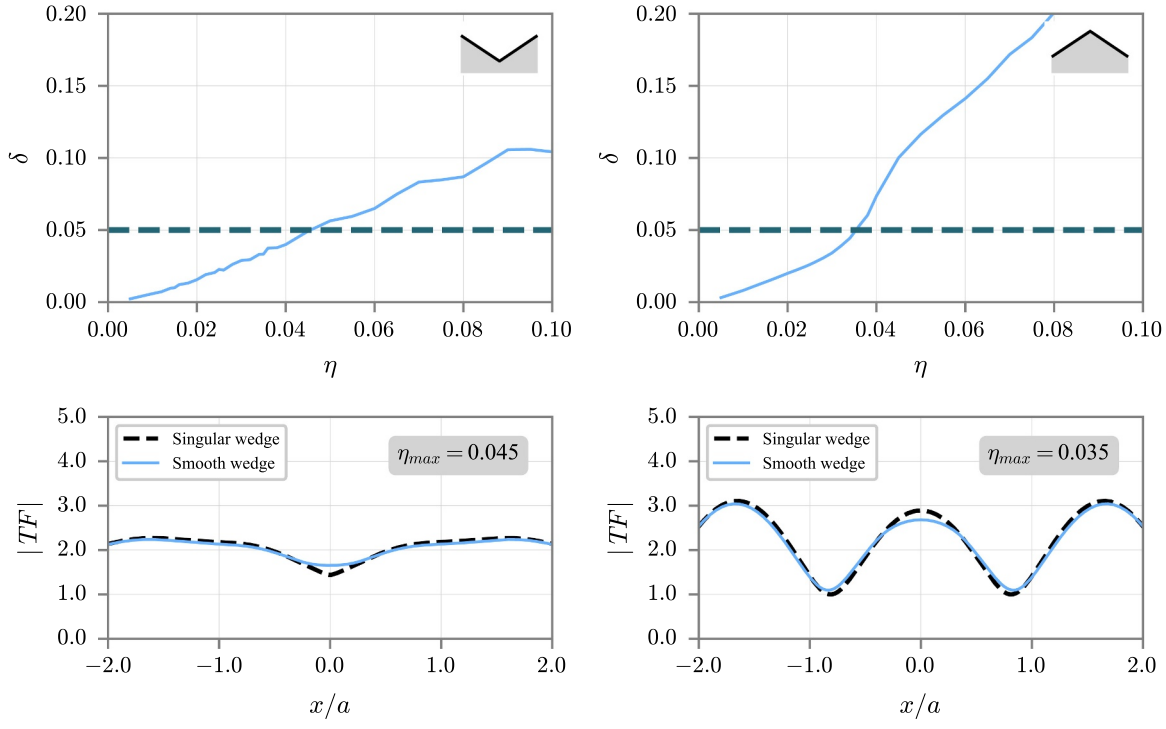

Fig. 3. The top part of the figure shows the variation of the error measure δ vs dimensionless frequency η in a concave and convex wedge under incident *SH* waves for a constant value of the slope angle $\alpha = 30°$. The dashed horizontal line intercepting the plot at η_{max} corresponds to the limit value of $\delta = 0.05$. The analysis was conducted with a boundary element method algorithm using 10 constant elements per wavelength with a shear wave propagation velocity $\beta = 1.0\ Km/s$ and mass density $\rho = 1.0$. The bottom part of the figure shows the spatial distribution of the amplitude function (TF) for the horizontal component of the displacement field from $-2a$ to $2a$ along the free surface of wedges (see Fig. 2). The TF is shown at a value of the dimensionless frequency corresponding to $\eta = 0.045$ in a convex wedge and $\eta = 0.035$ in the concave shape.

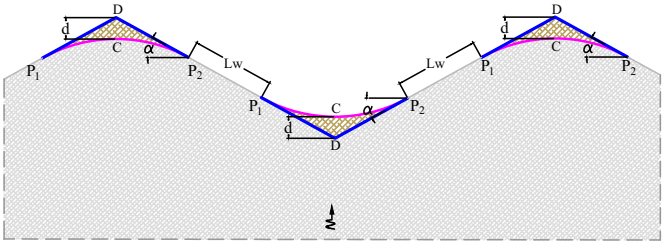

Fig. 4. Topographic irregularity conformed by two hills and a canyon resulting from the superposition of fundamental building blocks as those shown in Fig. 2. In this description the actual surface may resemble the singular wedge (blue line) or the continuous tangent curve (magenta line).

$$d = \eta \lambda^{tar} \tag{4}$$

and where we recognize the equivalence between h_{top}^{min} and d.

From the point of view of the wave propagation response, it follows that if we simultaneously represent a topographic profile with singular wedges D, or with tangent curves C, and the differences in the response are negligible, then all the topographic irregularities of dimension smaller than d are irrelevant to capture the response to the actual incident field. Therefore d is the characteristic dimension of the topographic element defined in Eq. (3) and setting the required level of topographic resolution.

3. Parametric analysis of topographic configurations

3.1. Error measure

Having recognized the distance parameter d (see Fig. 2) as the characteristic dimension of the fundamental topographic element on the basis of equivalent responses in the dual smooth-singular wedge approximation, it becomes evident that we require an objective measure to qualify and quantify the difference between both responses. As emphasized by η in Eq. (4) this is a frequency dependent problem. In this work we adopt as an appropriate error measure the differences in the frequency domain response obtained with each approximation. A quantitative assessment of these differences is defined in terms of the spatial distribution of the frequency domain amplitude function along the free surface of the singular and smooth wedge representation for a range of frequencies. Letting TF_{S_i} be the amplitude of the transfer function at point i obtained from the singular wedge approximation; TF_{C_i}= the amplitude of the transfer function at point i obtained from the smooth wedge approximation; and n= the number of observation points located from $-2a$ to $+2a$ along the free surface of the wedges (see Fig. 2), the error measure is defined as

$$\delta = \sqrt{\frac{1}{n}\sum_{i=1}^{n}\left(\frac{TF_{S_i} - TF_{C_i}}{TF_{S_i}}\right)^2}. \tag{5}$$

Using this error definition we now conduct several progressive parametric analysis intended to capture the admissible values of η for prescribed values of d and λ^{tar} in (4). Our study initially considers the simplest case of single, isolated convex and concave topographic elements and then increases complexity by extending the analysis to canonical shapes corresponding to trapezoidal-shaped canyons and hills.

In the first analysis, intended to capture the variation of the error parameter with dimensionless frequency, we considered convex and concave wedges under incident SH and SV waves for values of the slope angle α in the range [15°, 40°]. The analysis was conducted using an in-house implementation of the direct boundary element method [9] previously validated by [17]. A typical set of results, describing the δ vs η variation is shown in Fig. 3, while the complete set of responses is presented in the Appendix. We arbitrarily adopted the value of $\delta = 0.05$ as an acceptable limit for the error parameter. This is indicated in Fig. 3 by the dashed horizontal line intercepting the plot at the dimensionless frequencyη_{max}. That frequency corresponds to the maximum value of the η parameter in Eq. (4) for which both models predict equivalent results. Note that for those cases reported in the figure these values of η_{max} are $\eta = 0.045$ and $\eta = 0.035$ for a convex and a concave wedge respectively. The figure also shows the spatial distribution along the free surface of the amplitude function obtained with the singular and tangent curve representation of the wedge at the identified values of η_{max}.

3.2. Topographic interaction

The more realistic case of several adjacent elements (Fig. 4) brings into the problem the consideration of topographic interaction. We define topographic interaction as the perturbation introduced to the field produced by a topographic element A by the presence of a secondary element B. Since diffraction is frequency dependent and its amplitude decays with distance, it is intuitive to expect that this interaction is a function of the separation distance between topographic singularities. In the profile described in Fig. 4 this relevant and controlling parameter is the distance between points $P1$ and $P2$ in adjacent wedges and termed in this works as L_W.

The influence of L_W on the spatial variability of the response has already been identified by Jaramillo et al. [21] in the context of SH

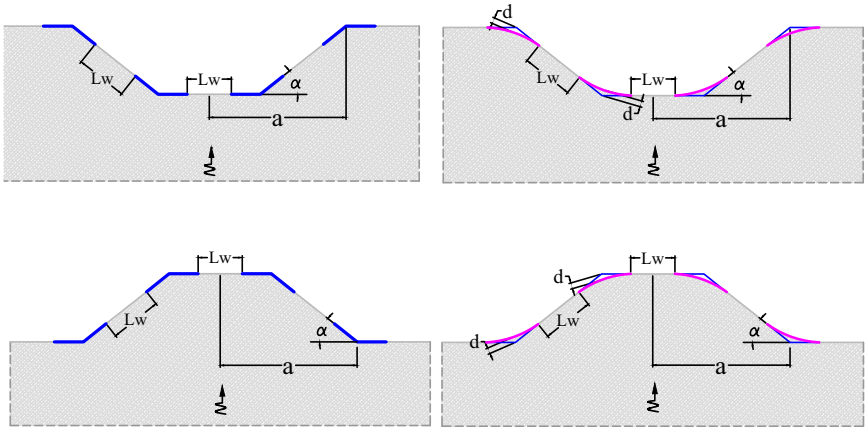

Fig. 5. Canonic forms corresponding to trapezoidal canyons and hills. Notice that V-shaped forms can be obtained as particular cases of the trapezoidal geometries. In this parametric analysis we tracked the variation in the error parameter δ vs dimensionless frequency η. First and second columns show the representation of the topographic feature in terms of singular and smooth wedges respectively. In each case the distance between topographic elements is L_W. The study was conducted over the following range of parameters $\alpha \in [15°, 40°]$, $\eta \in [0.005, 0.1]$ and $N = [1, 10, 25, 50]$.

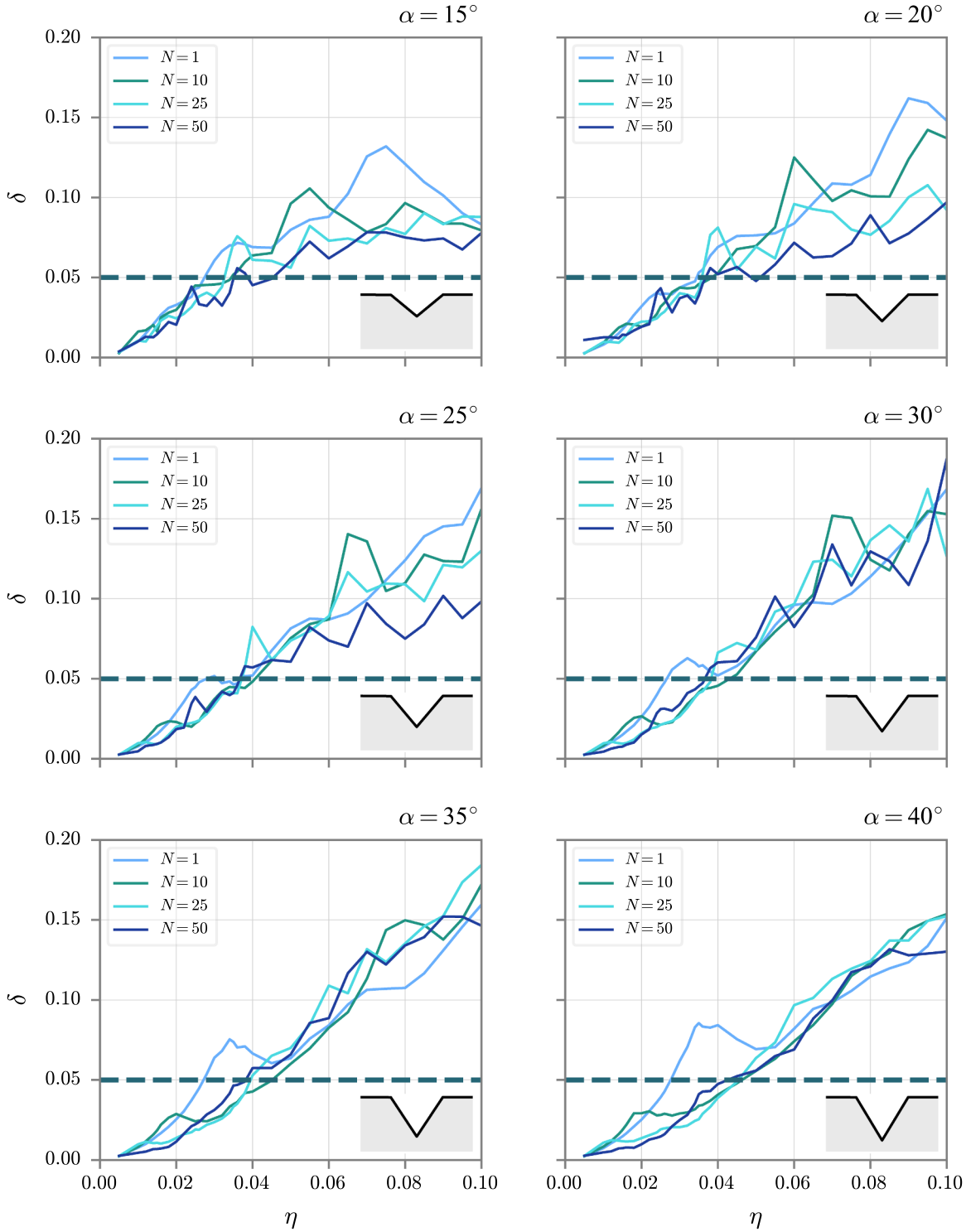

Fig. 6. Variation of the error parameter δ vs dimensionless frequency η in V-shaped canyons of slope angle α in the range $\alpha \in [15°, 40°]$ and subjected to incident *SV* waves. Each plot corresponds to a different separation between topographic elements as indicated by the parameter *N*. The dashed horizontal line intercepting each plot at the maximum frequency η_{max} indicates the acceptable limiting value of $\delta = 0.05$.

waves. In that work topographic interaction is defined as higher order diffraction and is identified in terms of cylindrical waves trapped between two adjacent singularities. With diffracted waves decaying with wave number the interaction between two wedges becomes important at low dimensionless frequencies. As the wavelength increases, the sources of diffraction are perceived by the incident field as being close to each other and although the interaction becomes stronger it takes place in the form of destructive interference resulting in an unmodified ground response. For instance, at low dimensionless frequencies a V-shaped canyon built by 3 perfect singular wedges is perceived by the incident field like a half-space with no topographic effect whatsoever. In the rest of this paper the parameter describing the distance between wedges is written as a factor of the topographic element size like:

$$L_W = Nd \tag{6}$$

and where *N* is a second dimensionless parameter relating the distance

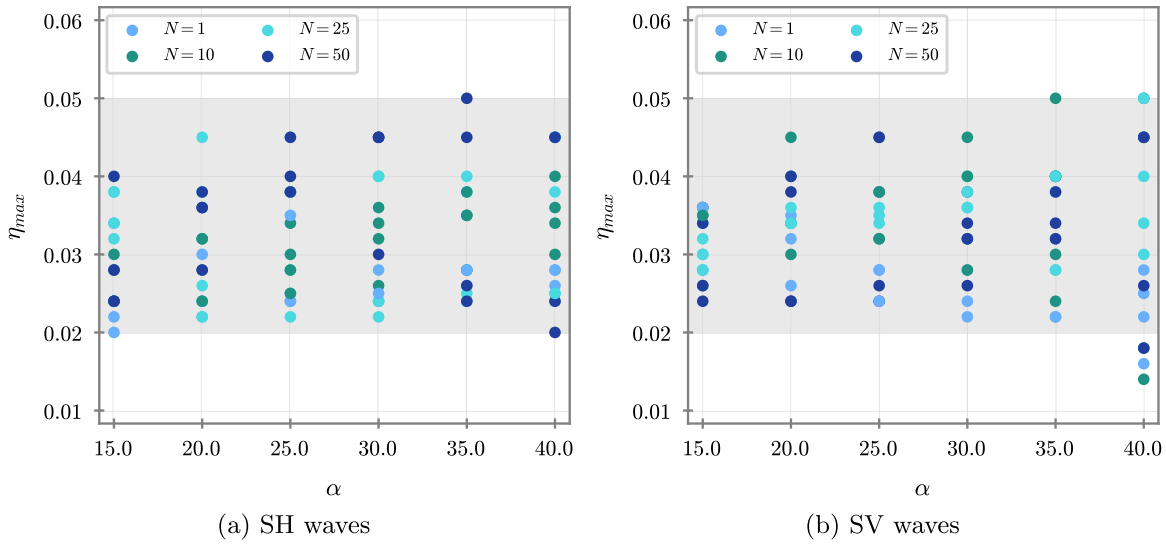

Fig. 7. Variation of the maximum dimensionless frequency η_{max} vs slope angle α for all geometries subjected to incident *SH* and *SV* waves and built with a superposition of topographic elements at different separation distances $L_W = Nd$. The 4 dots for a given color give the response for the 4 considered geometries, i.e., V-shaped canyons and hills and trapezoidal canyons and hills.

between wedges to the characteristic size of the topographic element *d*. The distance parameter L_W is paramount to the response of a topographic profile described as a superposition of wedges. This aspect of the response is further clarified by the analysis of a series of canonical topographies for different values of the described topographic parameters.

3.3. Response of canonical topographies

After emphasizing the fact that the geometric parameters d and L_W (or its dimensionless counterparts η and N), completely describe a generalized topographic profile, we now extend the parametric analysis over a set of canonical topographies in the form of trapezoidal and V-shaped canyons and hills (Fig. 5). These shapes can be easily constructed from superposition of topographic elements as those shown in Fig. 2. In this case, each geometric disturbance is defined by its slope angle α and by the geometric parameters d and L_W defining the conforming topographic elements. Notice that the V-shaped canyons and hills are particular cases of the trapezoidal geometries.

The analysis was conducted over the following set of parameters $\alpha \in [15°, 40°]$, $\eta \in [0.005, 0.1]$ and $N = [1, 10, 25, 50]$. The frequency domain response for the horizontal component of the displacement field from each resulting canonical shape under vertically incident *SH* and *SV* waves was evaluated using our implementation of the direct boundary element method. Typical δ vs η results for V-shaped canyons of different slope angles under incident *SV* waves are shown in Fig. 6 while the full set of results is presented in the Appendix. The main and most relevant output from each one of the studied cases displayed in Fig. 6, is the value of the dimensionless frequency η above which the error parameter δ reaches a value larger than the prescribed threshold of 0.05. This value is indicated by the point where the horizontal line intercepts theδ-curve. For subsequent reference this value has been labeled η_{max} and it is indicative of the maximum dimensionless frequency at which both approximations produce equivalent results. It is also observed from Fig. 6 that at $\eta < \eta_{max}$ the topographic interaction parameter N is of little relevance, while at $\eta > \eta_{max}$ the interaction becomes important in the shallow canyons (i.e., $\alpha = 15°$ and $\alpha = 20°$).

The variations of η_{max} with the slope angle α for all geometries resulting from the parametric analysis have been compiled in Fig. 7. Associated to each angle this plot shows the value of η_{max} for the 4 considered geometries and the 4 values of the interaction parameter N. It is observed that around 95% of the η_{max} values lie in the range $\eta_{max} \in [0.02, 0.05]$, so in order to formulate a proxy that can be used in the definition of the topographic element size associated to a prescribed target frequency we fixed the value of η in 0.02 and re-write Eq. (3) as:

$$h_{top}^{min} = 0.02\lambda^{tar}. \tag{7}$$

As a result, a model built in terms of dual smooth-singular elements and where all topographic irregularities with size smaller than the one predicted by (7) are eliminated would produce equivalent results.

With the definition of the fundamental topographic element and its objective description in terms of a dimensionless frequency parameter, we have introduced an analysis tool that can be used to make first order estimates of the expected frequency content in the response of a topographic scenario. Alternatively, the tool can be used to produce simplified representations of the topographic scenario as required by a target frequency. In this case the corresponding value of η_{max} can be used to find the required topographic resolution d that is needed to capture the response up to the target frequency.

To further illustrate the meaning of the dimensionless frequency parameter and its role in the effect of topography on the spectral response, we display in Fig. 8 (*SH* waves) and Fig. 9 (*SV* waves) the frequency domain amplitude function along the free surface of the V-shaped hill with slope angle $\alpha = 30°$ for the 4 considered values of the interaction parameter N. The top part in each figure shows the evolution of the error measure versus dimensionless frequency resulting from the parametric analysis. Each subsequent plot corresponds to the spatial distribution of the amplitude function for the maximum admissible value of the dimensionless frequency η_{max} taken from Fig. 7 according to each case. Notice that the maximum dimensionless frequency η_{max} is almost independent of the value of N and that a larger value of N is indicative of a larger number of wavelengths accommodated in the topographic profile.

4. Dynamic response of the Aburrá valley

The extensive analysis conducted over a wide range of parameters, including (concave and convex) geometries; slope angles; distance between diffraction sources; and wave types (*SH* and *SV* waves) has revealed that the dual singular-smooth wedge representation of the surface topography yields equivalent results up to a value of the dimensionless frequency $\eta = 0.02$. This result also implies that, all the topographic irregularities of characteristic dimension:

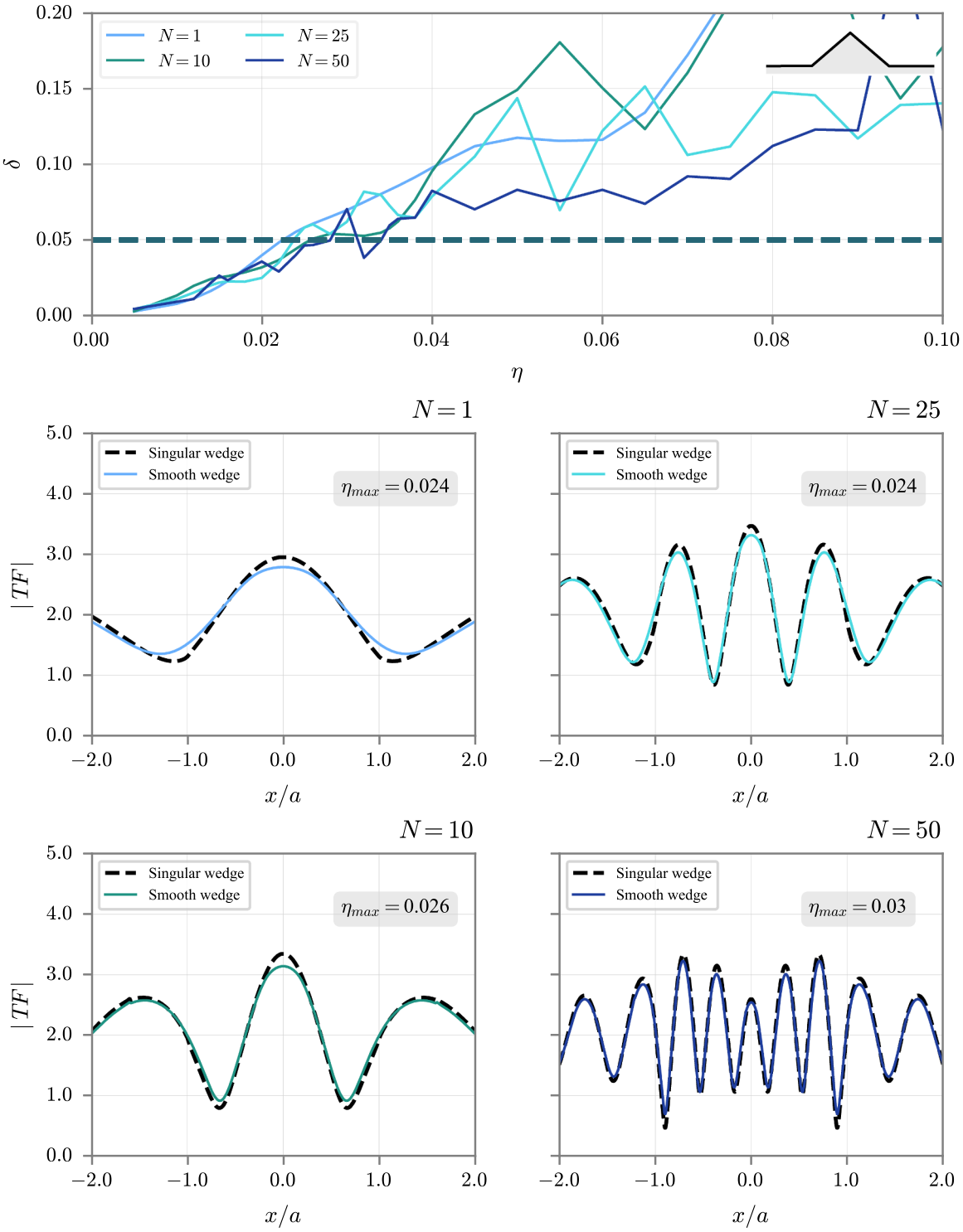

Fig. 8. Spatial distribution of the amplitude function along the free surface of V-shaped hills of slope angle $\alpha = 30°$ under incident *SH* waves at constant values of the dimensionless frequency η. Each panel shows the results for the model built with the singular and smooth wedge representation with distance between wedges L_W. The dimensionless frequency in each case is taken from Fig. 7 and corresponds to the point where the dashed horizontal line intercepts the δ vs η curve in the top panel of the figure.

$$h_{top}^{min} < 0.02\beta T^{tar} \tag{8}$$

forming a surface profile in a medium of shear wave propagation velocity β, are irrelevant if the spectral response is expected to be accurate as prescribed by the target period T^{tar}. In this section we apply these ideas to the evaluation of the dynamic response of the Aburra Valley Region (AVR) in Medellin, Colombia. This is a long-shaped sedimentary basin located at the north end of the central range of the Colombian Andean region in Northwestern South America. For a brief description of the prevailing tectonic environment the reader is referred to Restrepo et al. [33]. The valley has a total length of about 30 *km* and a shortest width of about 7 *km* near its center. Most of the basin is occupied by residual soils and hill-slope deposits, which are susceptible to seismic wave amplification due to local effects. The eastern part of the region is dominated by moderate to steep slopes (>30 per cent) with geometric irregularities of various lengths. The city of Medellin (second largest

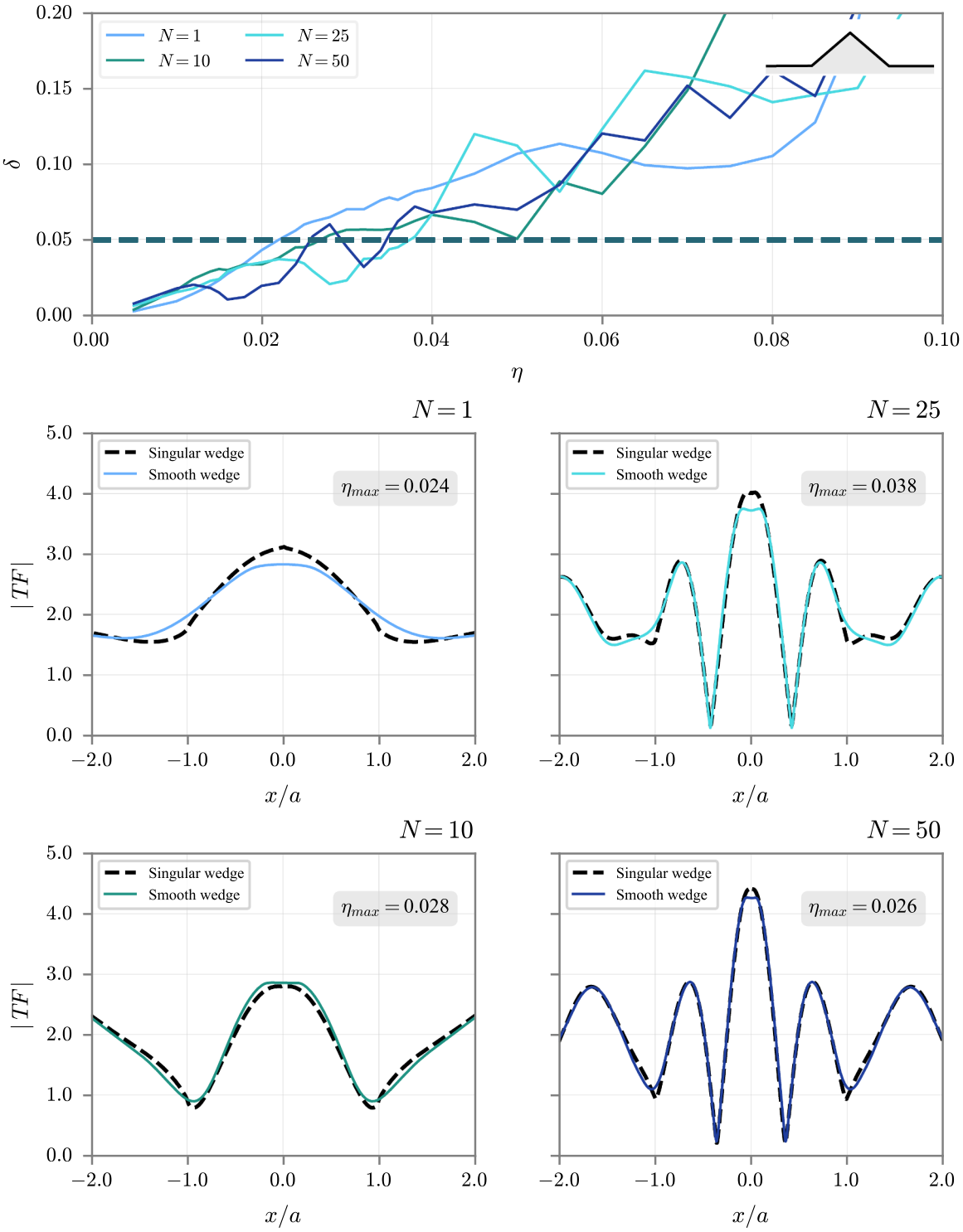

Fig. 9. Spatial distribution of the amplitude function along the free surface of V-shaped hills of slope angle $\alpha = 30°$ under incident *SV* waves at constant values of the dimensionless frequency η. Each panel shows the results for the model built with the singular and smooth wedge representation with distance between wedges L_W. The dimensionless frequency in each case is taken from Fig. 7 and corresponds to the point where the dashed horizontal line intercepts the δ vs η curve in the top panel of the figure.

city in Colombia with nearly 2.5 million habitants) occupies most part of the valley. In addition to this complex topographic scenario its south-east sector has seen a tremendous growth in population during the last 30 years with an architectural setting composed mostly by mid to high rise reinforced concrete buildings with fundamental periods larger than 2.0 s. Colombian seismic regulations allow for the implementation of local site effects through particular studies as an alternative to the mandatory site coefficient approach based upon the 30 m soil classification. However in these regulations there are no specific guidelines as to how to consider possible topographic effects if any. Topographic effects for this scenario have already been addressed by Restrepo et al. [33] using large scale computational models considering the seismic fault and a first version of a community velocity model for the city. That work revealed a strong modification to the incident wave field induced by topographic effects. Here we will concentrate not in the accurate prediction of the ground motions considering mechanical

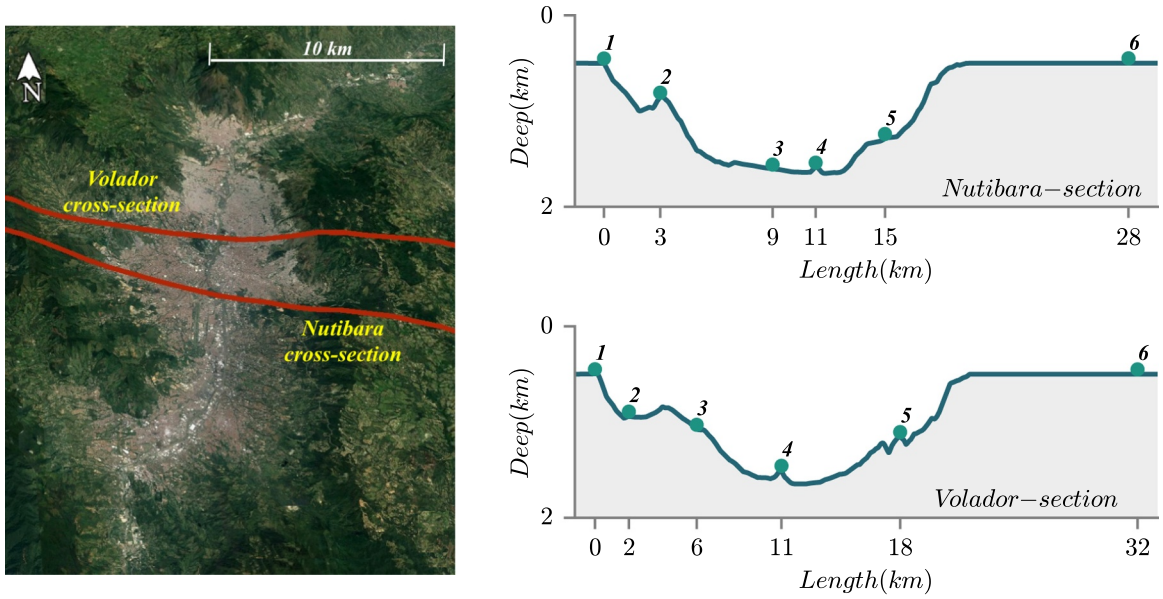

Fig. 10. Overall view of the dominant surface topography in the AVR. The shaded rectangles correspond to the two west-east cross sections analyzed in this work. Both sections contain a localized topographic feature in the form of an isolated hill in the center of the valley and a stronger coupled topography towards the east and west margins. In both cases the slopped parts of the topographic scenario are highly populated with a large density of reinforced concrete buildings with varying quality levels.

Table 1
Physical description of the receiver points considered in the studied cross sections.

Feature	Name	Receiver	Cross section
	Diffractor	①	CN, CV
	High frequency canyon	②	CV
	High frequency hill	②	CN
	Flat open	③	CN
	Long slope	③	CV
	Isolated hill	④	CN, CV
	Flat closed	⑤	CN, CV
	Halfspace	⑥	CN, CV

and geometrical effects, but only in the determination of the modifications experienced by the incident motions due to the overall surface topography. Moreover, the main goal in our analysis is to test and highlight the connection between topographic resolution and spectral response and to explore its potential application to site response analysis. It must be recognized that previous results from other groups have shown that there might be a strong, non-linear coupling between mechanical and geometric effects, [6]. However, a model based on single-material properties might still be valid for topographic effects if the differences in stiffness between the existing soil deposits is small.

In this study we will focus in the response at two cross sections involving localized topographic features and interacting topography. Fig. 10 shows the overall topographic scenario dominating the AVR and the two cross sections of interest. In general, both sections are representative of the topographic layout prevailing in the region with soft slopes, or even an almost flat configuration, in the center of the valley with steeper slopes in the west and east flanks. The east margin is particularly important as it continues its extension along a second flat region (not shown in the figure) with an increasing growth in population. The figure also displays the topographic profiles existing at each cross section. Points marked ①through ⑥indicate receivers for further analysis. The first section contains an isolated hill, named Cerro Nutibara, located at the bottom of the valley (receiver ④). This formation has a shape closely resembling that of a trapezoidal wedge of approximate height $h = 120,\ m$. Cerro Nutibara (CN) section also contains a smaller isolated hill over the west flank (receiver point ②) and a flat step-like site over the east flank (receiver point ⑤). This last site is characteristic of artificial formations introduced during typical construction process. A second flat site has also been selected at the bottom of the valley (receiver point ③), locally approaching half-space conditions as the flat geometry is enclosed by the lateral boundaries defining

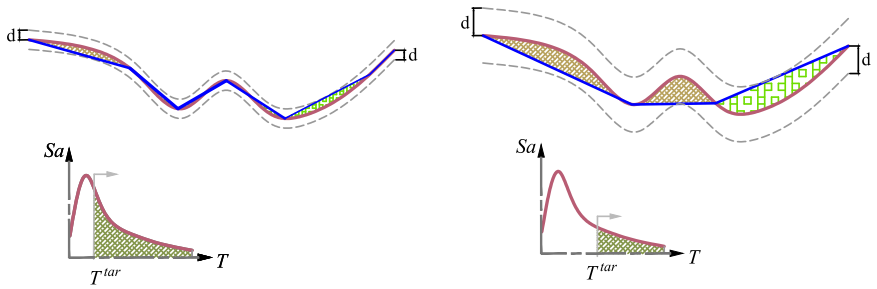

Fig. 11. Schematic description of a topography-dependent-response-spectra (*TRS*). The target structural period T^{tar} sets the size h_{top}^{min} of the minimum topographic element that must be retained in the computational model in order to predict results accurate in the shaded period range. The topographic features inside the band of size $\pm\ d$ are eliminated by the singular wedge approximation. Smaller sizes for the minimum topographic element implies an increase in accuracy in the response spectra.

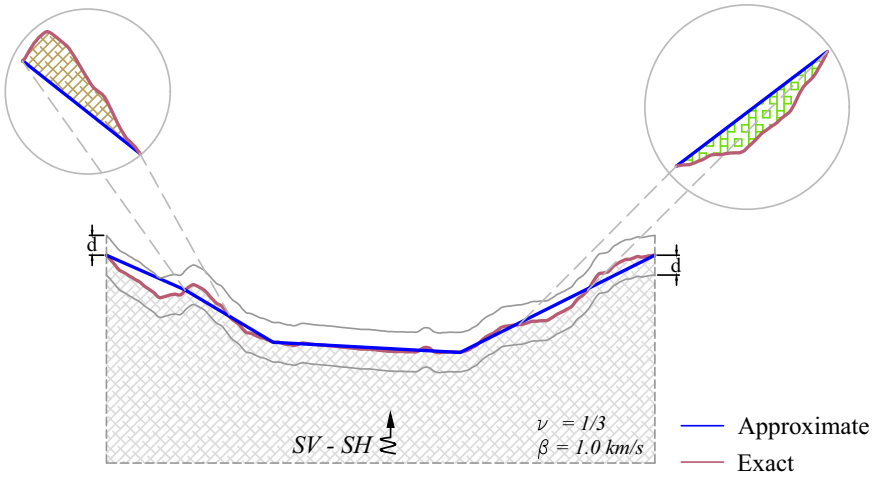

Fig. 12. The topographic irregularities contained within the band of size ± d surrounding the original topographic profile are irrelevant for the model intended to predict accurate results up to the target frequency f^{tar}. The blue line marks the topographic irregularities of characteristic dimension larger than d as per Eq. (7). This final model can be analyzed with standard numerical techniques in order to predict the response up to the target frequency f^{tar}.

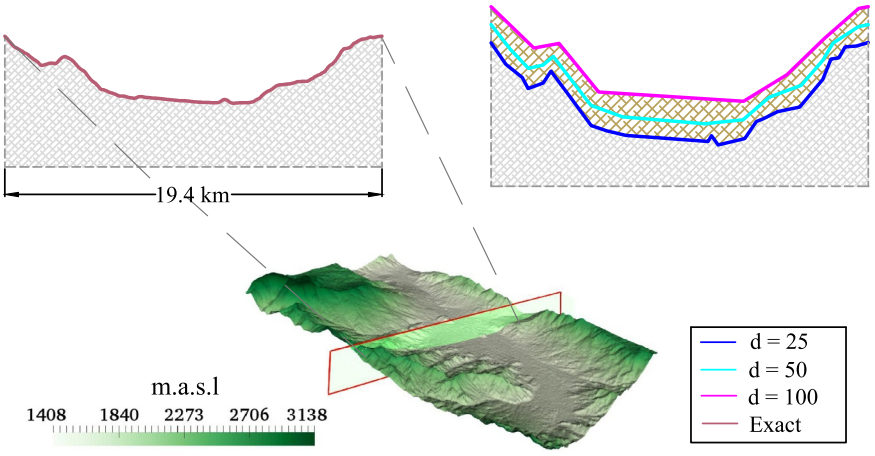

(a) Nutibara cross section

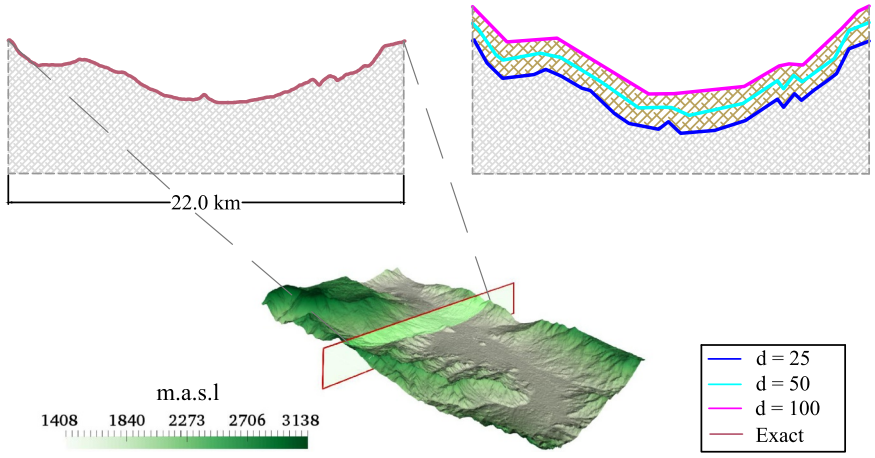

(b) Volador cross section

Fig. 13. Complete and effective cross sections at the CV (top) and CN (bottom) formations after applying the band simplification algorithm with topographic element parameter $h_{top}^{min} \equiv d = [25.0,\ 50.0,\ 100.0]\ m$.

the slopes of the valley. The second cross-section under analysis contains also an isolated hill, known as Cerro Volador (CV), with a trapezoidal shape of approximate height $h = 180,\ m$ (receiver point ④) and located at the bottom of the valley. By contrast with CN-section, this formation contains a small depression in the west flank with a form closely approximating that of a V-shaped canyon (receiver point ②).

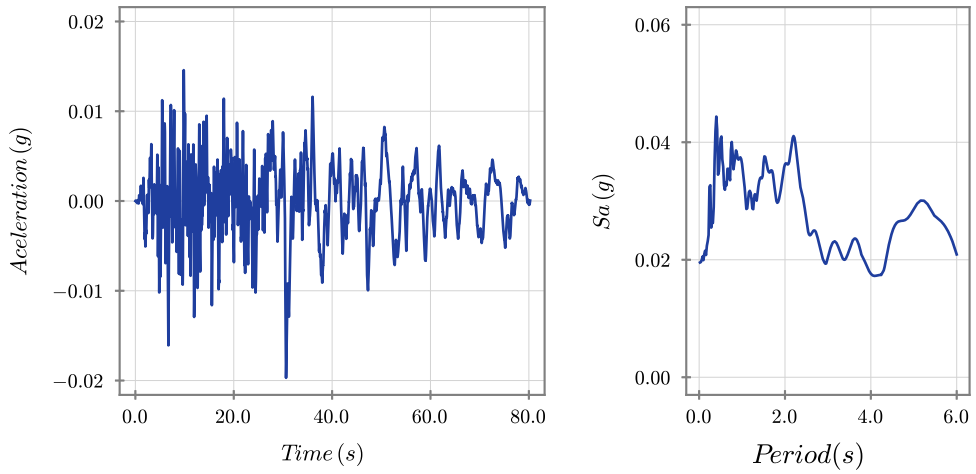

Fig. 14. Acceleration time history and response spectra for the N-S component of the Manchester station record corresponding to the 1999-Hector Mine earthquake.

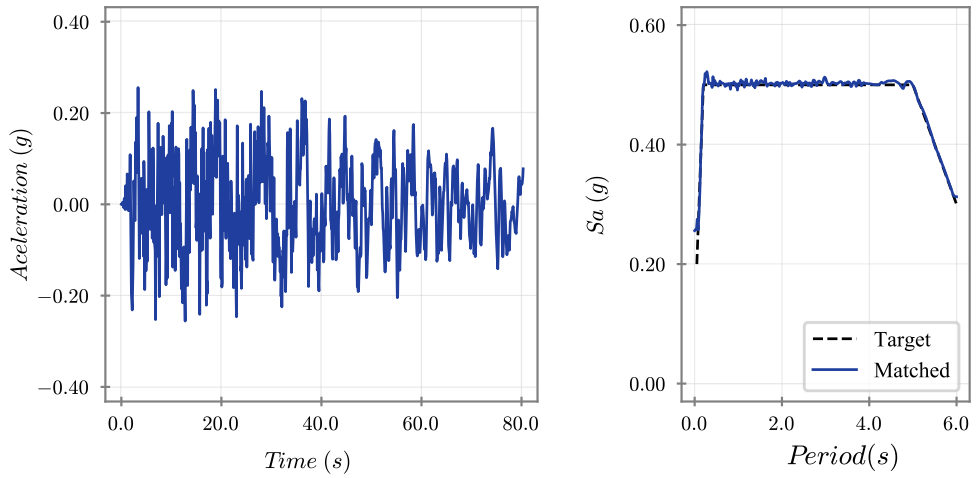

Fig. 15. Acceleration time history and response spectra corresponding to the synthetic signal used in this study. The target response spectra corresponds is shown by the dashed line.

Towards the east margin the cross section includes a second small-scale hill (receiver point ⑤) as opposed to the flat feature considered in CV-section. We have also included a flat site located over the west flank (receiver point ③). This last point is intended to produce results comparable with those at point ③in CN-cross section. In addition to the previously described set of receivers, both models consider also a diffraction source located along the top part of the west margin (receiver points ①), and a half-space point located over the east, in the region identified as San Nicolas valley (receiver points ⑥). The considered cross sections and selected receivers are expected to represent topographic effects in a wide frequency regime and introduce different types of spatial motion variation. Table 1 presents a physical description of the different receivers along both cross-sections.

4.1. Spectral response considering topographic effects

Each one of the two cross sections of the AVR was represented by simplified topographic models after applying the ideas developed in the previous sections of this article. To obtain different topography-limited-response-spectra (*TRS*) we built simplified models using topographic elements of different characteristic dimensions. Note that in this work a topographic element is a conceptual physical parameter associated to a particular topographic scenario. As a result, in the construction of simplified models we can remove but we cannot add new topographic elements. This implies that the difference between two models of the same scenario lies in the number and size of topographic features that are retained in each case. In the computation of the *TRS* we prescribed values of the target period corresponding to $T = [1.25, 2.5, 5.0]\ s$, implying topographic elements of characteristic size of $d = [25.0, 50.0, 100.0]\ m$. These were computed using $h_{top}^{min} = 0.02\beta T^{tar}$ with $\beta = 1.0\ km/s$. The value of $\eta = 0.02$ corresponds to the lower bound of maximum dimensionless frequency as per the parametric analysis.

To construct the simplified models we used the previously found result that for a given target period T^{tar} the value of d specified by Eq. (7) allows us to remove (or modify) all the topographic irregularities of size $\ell < d$ without altering the response spectra at periods larger than T^{tar}. This condition can also be understood to imply that, within a band of size $2d$, built parallel to the original topographic profile at a distance $\pm\ d$, an approximation in terms of straight lines (i.e., singular wedges) predicts the response accurately up to the target period T^{tar}. The detailed procedure is schematized in Fig. 11, where the red line represents the actual profile and the band of width $2d$ is shown by dashed lines separated by a distance $\pm\ d$ from the actual surface. Inside this band we now approximate the actual topography in terms of straight (blue) lines forming singular wedges. Note that these straight lines would eventually smooth out all the topographic features contained inside the band and therefore smaller than d. Clearly as the band size is reduced the model approaches the actual topography and increases the accuracy of the *TRS* as shown by the dashed portion of the schematic response spectra in each case.

To bring into attention an additional aspect of the approach we

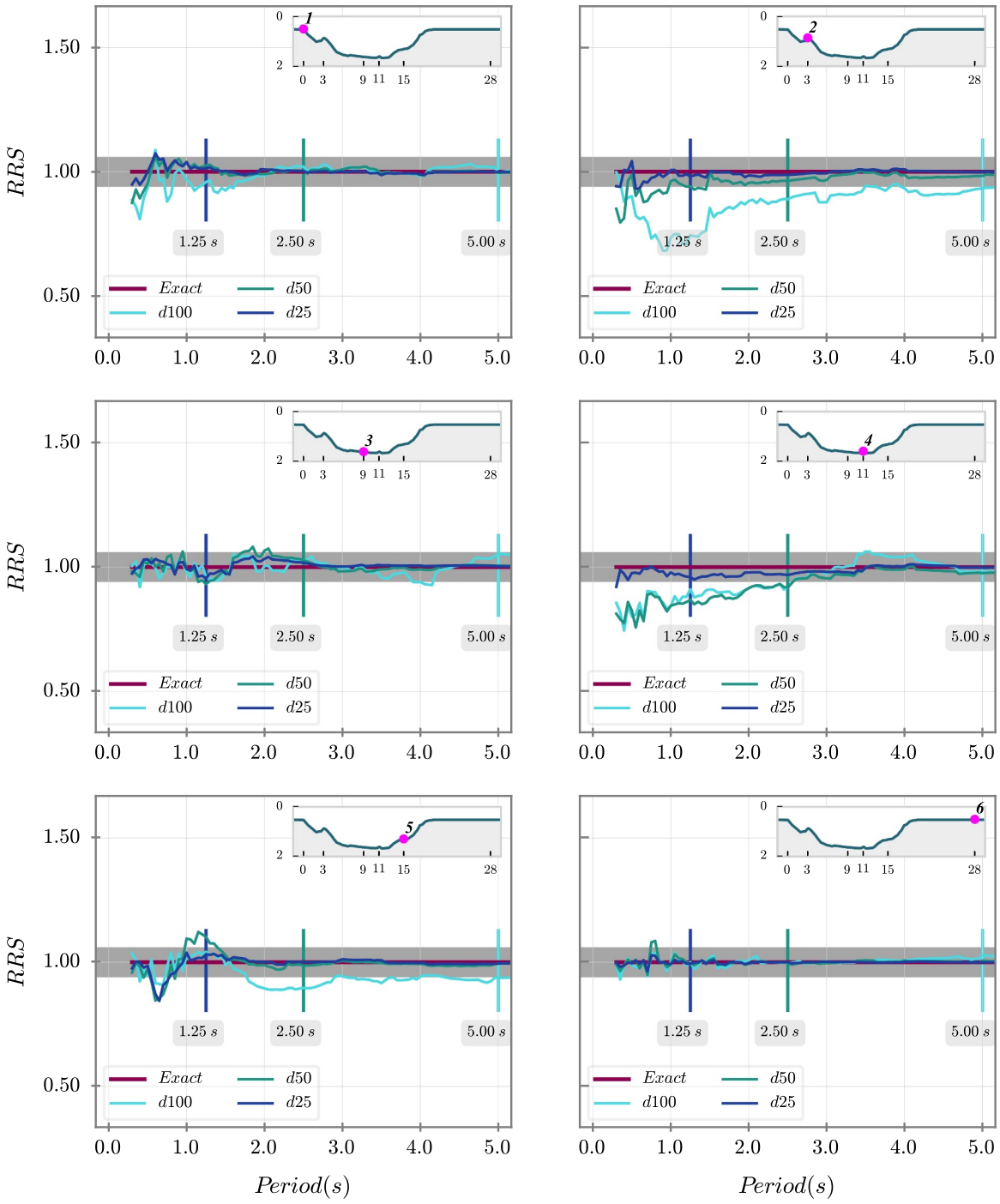

Fig. 16. Ratios of response spectra between the results from the modified models corresponding to values of the resolution parameter d = [25, 50, 100] m as per Eq. (7) and the exact topographic representation for the 6 receiver points in the Cerro Nutibara cross section under vertically incident *SV* waves. The vertical line in each plot corresponds to the value of the target period for each value of d.

show in Fig. 12 a complete topographic profile and the parallel band of size $2d$. Notice (as shown by the zoomed-in insert figures) that the artificial profile (shown in blue) may remove (or add) concave and convex relief. This schematic description of the analysis method makes evident that the approximate solution (blue line) within a given band is not unique, as different topographies may be proposed. Despite of this possibility of multiple solutions the approach is accurate as these differences would only produce modification at periods smaller than T^{tar}.

To clarify this methodological aspect of the approach, assume that the analyst is interested in finding an accurate response spectra in a period range between 1.25 s and 5.0 s. Setting T^{tar} = 1.25 s in Eq. (8) together with β = 1000 m/s we obtain a minimum value of the topographic element h_{top}^{min} = 25.0 m. This value of the required topographic resolution is later used in the construction of the simplified model. This is achieved by drawing two auxiliary surface profiles parallel to the actual topography at a distance ± 25 m. Within this resulting band of width $2d$ = 50 m (see Fig. 12) any model built in terms of straight lines forming wedges provides results with the expected accuracy in the response spectra. These set of values was used in the construction of the d = 25 m-model used in the analysis of the AVR.

Fig. 13 shows the two cross sections studied in this research. The shaded box shows the relative location of the section within the

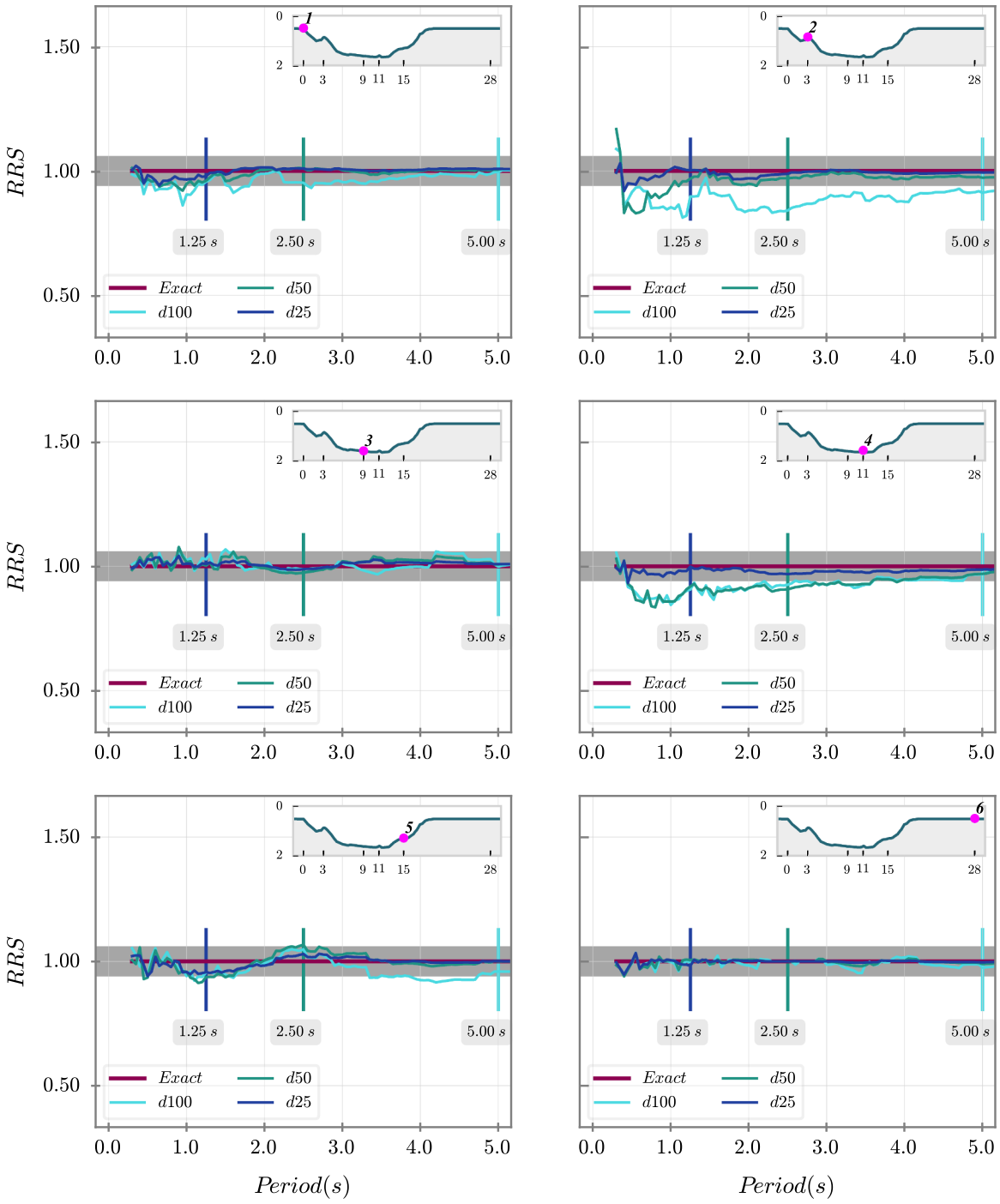

Fig. 17. Ratios of response spectra between the results from the modified models corresponding to values of the resolution parameter d = [25, 50, 100] m as per Eq. (7) and the exact topographic representation for the 6 receiver points in the Cerro Nutibara cross section under vertically incident *SH* waves. The vertical line in each plot corresponds to the value of the target period for each value of d.

complete AVR. The complete original profile is shown in the left top part of the figure while the 3 modified models corresponding to topographic elements of size d = [25.0, 50.0, 100.0] m are shown in the top right of the figure.

At each cross section we found the horizontal displacement component of the response corresponding to the exact topography and to the three simplified models for vertically incident *SH* and *SV* waves using our previously referred boundary elements scheme. The boundary element implementation satisfies exactly radiation boundary conditions at infinity and applies the plane wave excitation in terms of effective motions so our results are accurate up to numerical round-off errors. To obtain a time domain representation of the response, we computed synthetic seismograms as input motions after using a seed and a target response spectra. The seed consisted of records from the horizontal component at the Manchester station corresponding to the Hector Mine earthquake (Fig. 14). These seeds were modified using the wavelets algorithm from Al Atik and Abrahamson [3] to produce maximum response spectral amplitudes in a period range between 0.5 s and 6.0 s (Fig. 15). These artificial motions are tailored to a wide band response spectra in such a way that it would allows us to identify amplification (or reduction) levels over a large period range.

Figs. 16 to 19 display the results for both cross sections along the 6

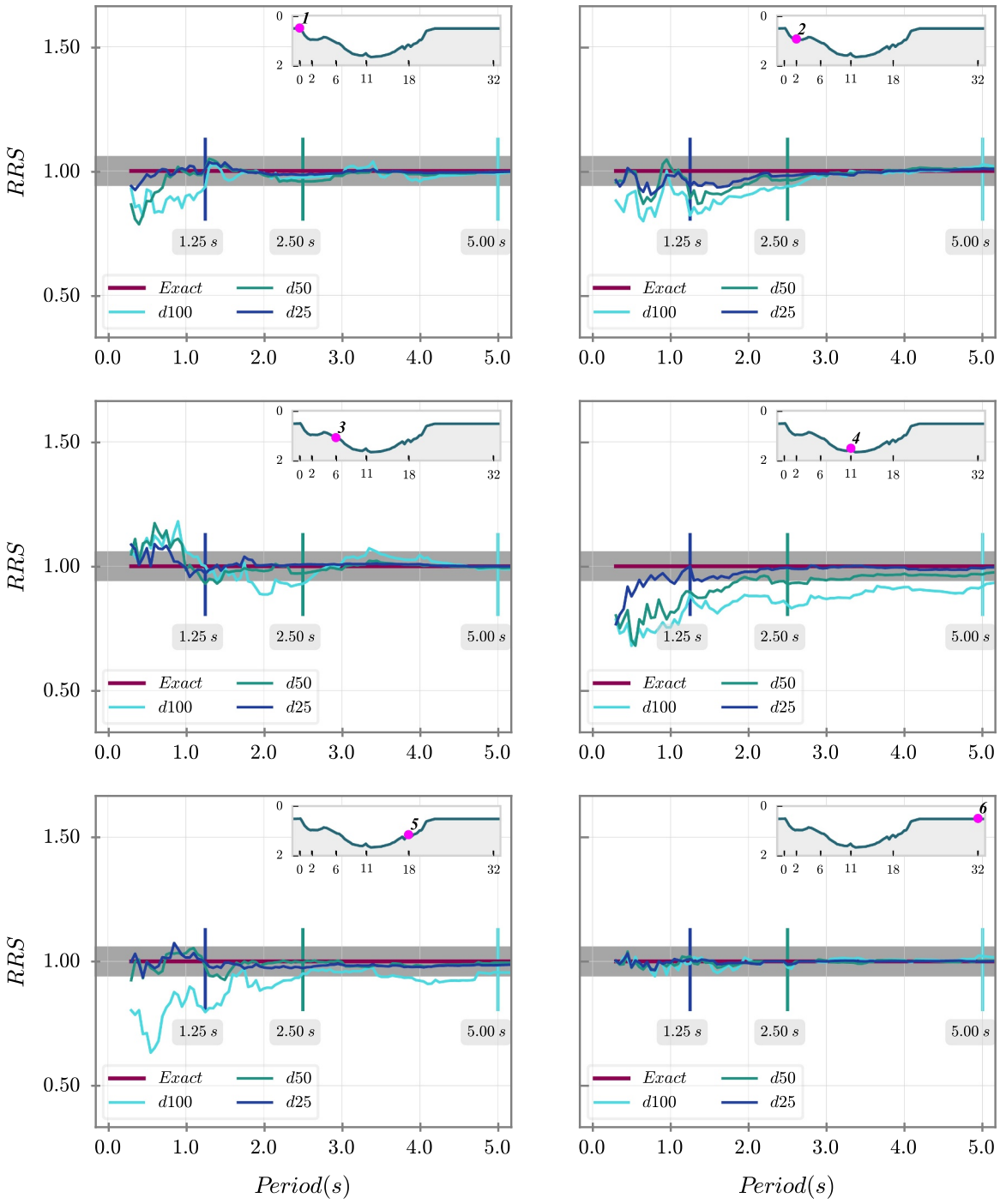

Fig. 18. Ratios of response spectra between the results from the modified models corresponding to values of the resolution parameter d = [25, 50, 100] m as per Eq. (7) and the exact topographic representation for the 6 receiver points in the Cerro Volador cross section under vertically incident *SV* waves. The vertical line in each plot corresponds to the value of the target period for each value of d.

receiver points when the models are subjected to vertically incident *SV* and *SH* waves. The results are presented in the form of spectral ratios (or ratios of response spectra *RRS*) between the response obtained with the simplified models and the one for the exact topography. Each panel shows the response at one of the 6 receivers points as indicated in the insert figures (see Fig. 10). In each case the vertical lines in the *RRS* indicate the prescribed target period associated to each value of d. On the other hand, the small gray band surrounding the *RRS* results corresponds to the 5.0% acceptable error. This implies that the portion of the *RRS* contained within this gray zone is assumed to be accurate. It is observed that in all cases accuracy is obtained up to the target period and in almost every case this accuracy is even extended towards the lower period range. Notice that the reported *RRS* results are not indicative of the presence or absence of topographic effects but to the quality of the response from the simplified model with respect to the exact profile. In this sense a value of 1.0 in the *RRS* plot corresponds to exact prediction of the response.

The results in terms of the *RRS* s show that the response obtained with the simplified models at receivers corresponding to flat topographies (i.e., receivers ③and ⑥with physical conditions indicated by ⏦ and ⊖ respectively) are accurate nearly over the complete frequency range. This is an obvious and expected result since at these

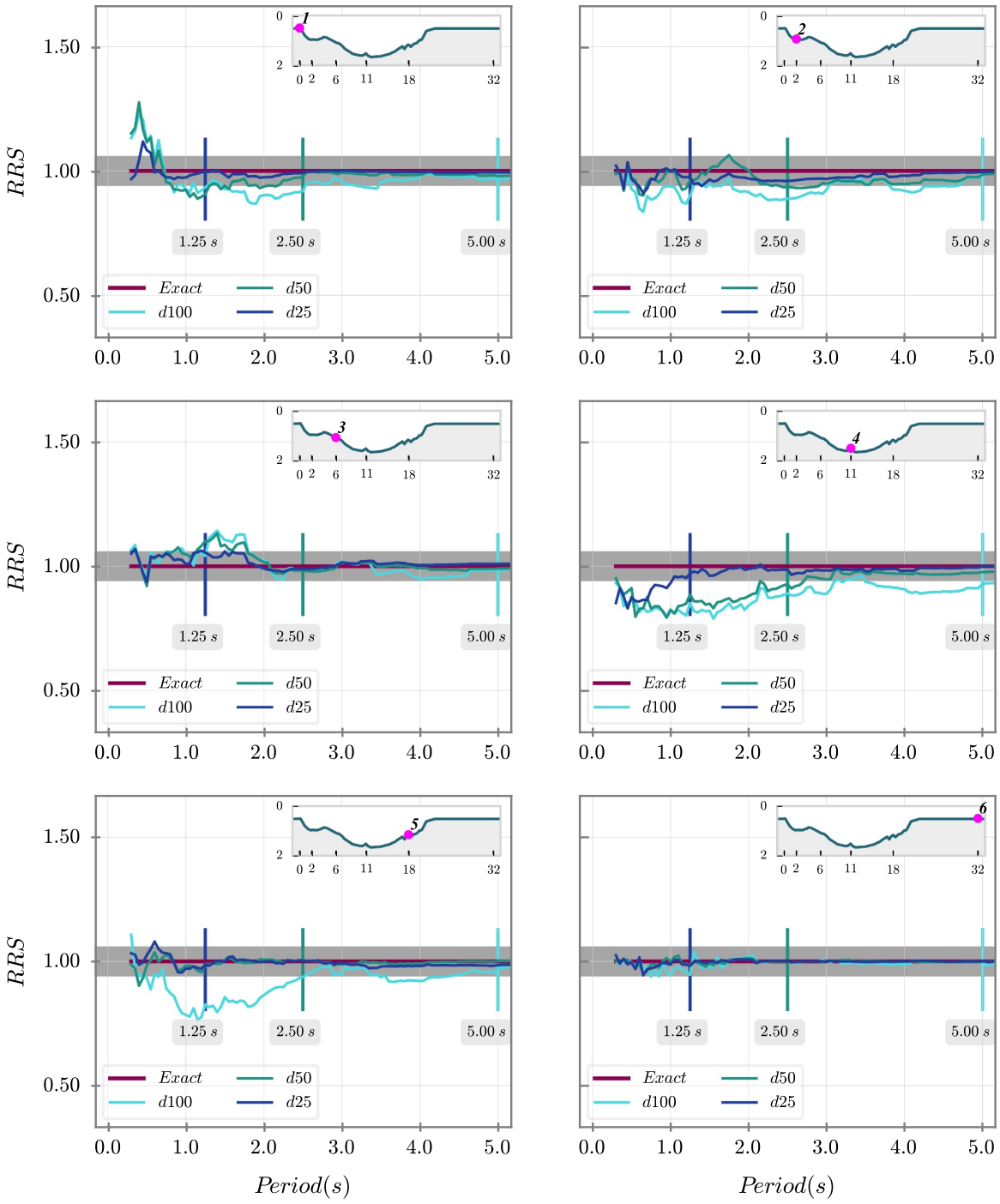

Fig. 19. Ratios of response spectra between the results from the modified models corresponding to values of the resolution parameter $d = [25, 50, 100]$ m as per Eq. (7) and the exact topographic representation for the 6 receiver points in the Cerro Volador cross section under vertically incident *SH* waves. The vertical line in each plot corresponds to the value of the target period for each value of d.

locations there are no local irregularities to be removed by the approximate models. At receivers with isolated topographies, like points ④with physical conditions denoted by ⌒, the exact response is predicted by the $d = 25$ m-model, while models corresponding to $d = 50$ m and $d = 100$ m are accurate for periods larger than $T = 2.5$ s and $T = 5.0$ s respectively. It must be observed that these points might be considered isolated as there are no additional nearby formations generating wave interaction. By contrast, in the case of local topographies of smaller size, like receiver ②in CN-section with physical conditions indicated by ⌒, the $d = 100$ m-model fails to predict the response in periods larger than $T = 5.0$ s, while at the same point in the CV-section, where the local geometry takes the form of a V-shaped canyon, the three models predict accurate results. As a final observation the response at the major diffraction sources (i.e., receivers ①with physical conditions ⌒) and those corresponding to half-space conditions (i.e., receiver ⑥) the response is fully captured by the $d = 25$ m and $d = 50$ m models. At the diffraction source this can be explained in terms of the smoothing introduced in the simplified models and the fact that nearby smaller topographies are effectively removed. To summarize our results, it is clear that for the AVR the response over the complete frequency band is fully captured by simplified models with topographic elements corresponding to $d = 25$ m. However if the analyst is

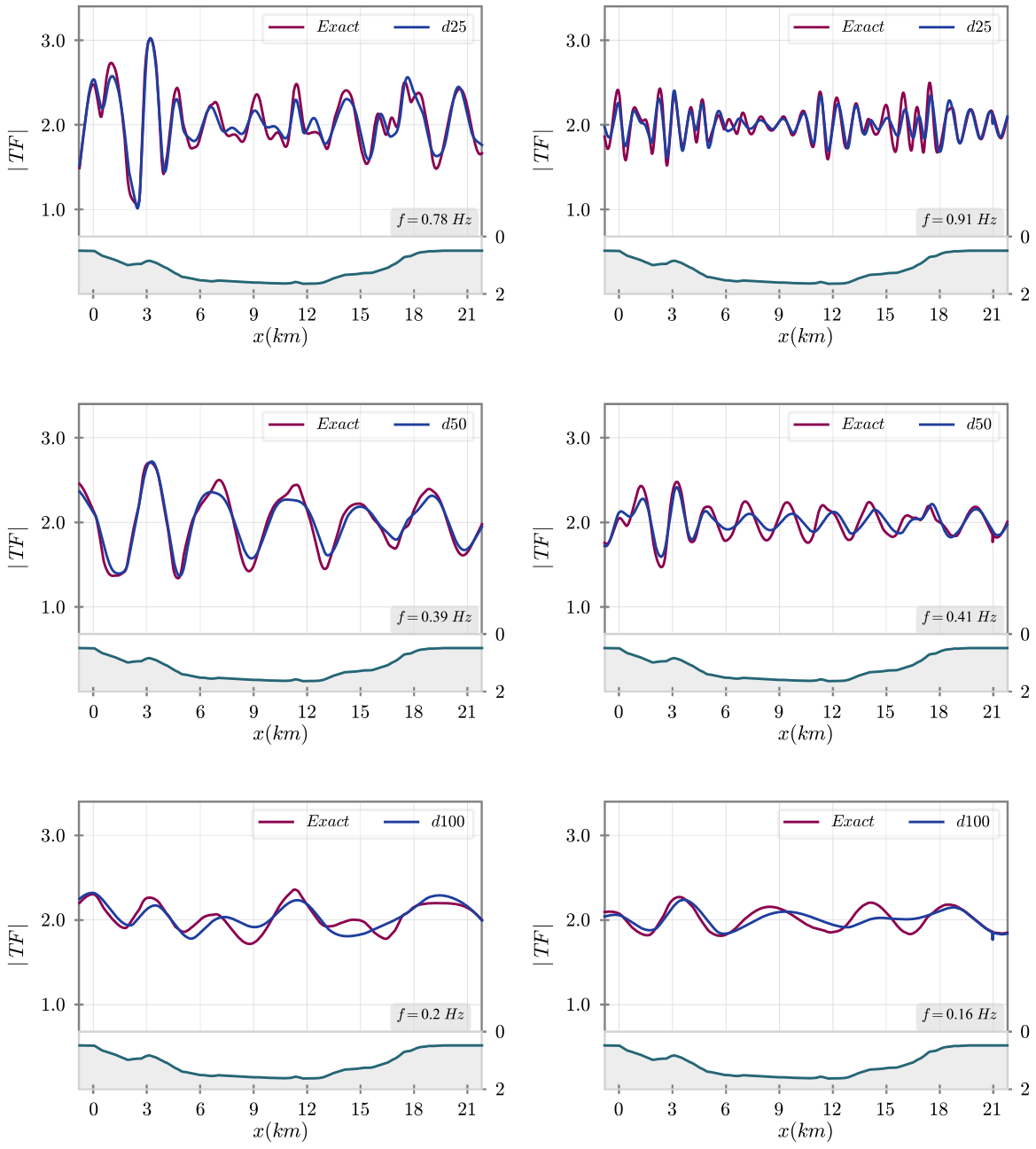

Fig. 20. Comparison of the spatial distribution of the frequency domain amplitude function along the free surface for the original and simplified profiles in the Cerro Nutibara cross section. Left and right columns are for *SV* and *SH* waves respectively.

interested in periods larger than $T = 5.0\,s$ the topographic resolution can be as low as $d = 100\,m$.

As a complementary result, Fig. 20 and 21 compare the spatial distribution of the frequency domain amplitude function (TF) along the free surface of each cross section for the exact and modified profiles respectively. Left and right columns show the response for *SV* and *SH* waves for a target frequency associated to a value of the error parameter $\delta = 0.05$.

Besides the observed match between the *RRS* and *TF* solutions, the results also reflect the importance of surface topography for ground motions in the low frequency range. For instance, it must be emphasized how the response in the 5.0 *s* period is modified by topography in a regional scale (order of kilometers) while an adequate topographic response at a local site requires the consideration of topography in a local scale (order of meters) affecting the spectral response in lower periods.

5. Conclusions and further work

We have studied the influence of surface topography in the problem of site effects in earthquake engineering. Using a generalized infinite wedge as a fundamental building block in the representation of an arbitrary surface topography, we introduced the concept of topographic resolution as the frequency range that can be effectively propagated through a given topographic profile. This was achieved after assigning a characteristic dimension to the otherwise dimensionless wedge, thus defining a generalized topographic element. Such definition of topographic resolution in terms of the size of the topographic element was later used to establish a physical connection between the geometrical features existing in a topographic scenario and the resulting spectral response of the profile. The physical connection was calibrated via parametric analysis of infinite wedges and of canonical shapes (canyons and hills) with concave and convex geometries. Using these ideas we

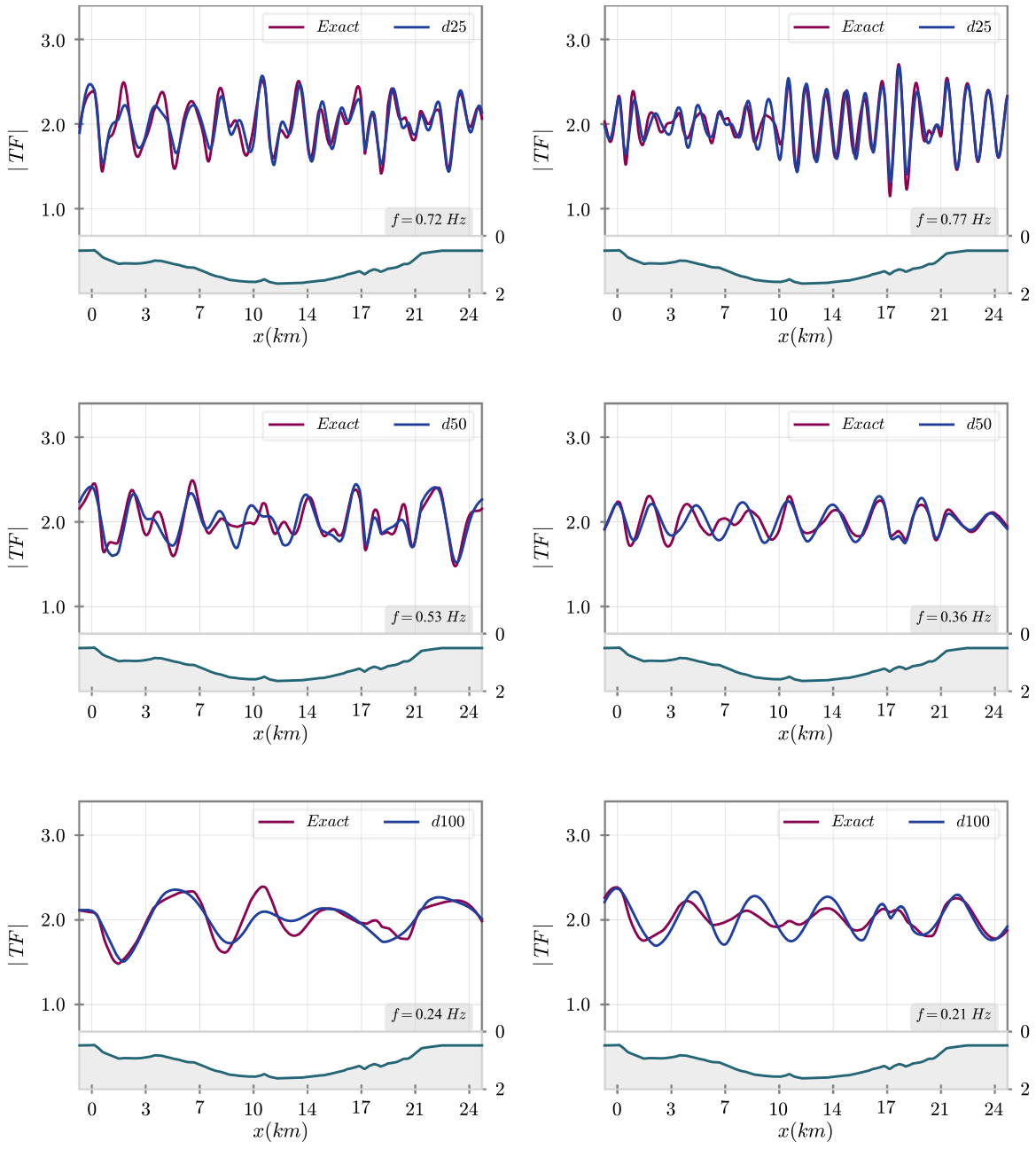

Fig. 21. Comparison of the spatial distribution of the frequency domain amplitude function along the free surface for the original and simplified profiles in the Cerro Volador cross section. Left and right columns are for *SV* and *SH* waves respectively.

proposed a rational technique to make first order estimates of the expected frequency content associated to a given topographic scenario. These same ideas can also be used to guide the analyst in identifying which geometric features of a given topographic scenario are relevant in the estimation of the ground motions at a local site if the analysis is expected to accurately capture the response up to a target period: such partially accurate response spectra is henceforth termed topography-limited-response-spectra (*TRS*). To test the established physical connection between the spectral response and the geometric features of the topographic profile we conducted analysis for the Aburr Valley Region (AVR) in Medellin, Colombia. To that end we defined 3 target periods representative of typical reinforced concrete buildings in the region and determined 3 different models which resulted after eliminating the unnecessary topographic features in the profile. The analysis were conducted for two cross sections of the AVR comprising geometric irregularities of various physical conditions. A comparison between the spectral responses obtained with the exact and simplified topographies showed that in fact the response spectra resulting from the simplified models accurately predicts the response at least up to the target period and in many cases at even lower values. Although we are well aware of the fact that the modifications to the incident seismic field are the result of several combined effects like mechanical impedance and surface and sub-surface topography, this work contributes to the understanding of the challenging problem of geometric effects in earthquake engineering.

The analysis of canonical topographies and of the realistic scenario corresponding to the AVR have emphasized the role, as controlling parameters in the topographic effect, of the characteristic size of the topographic features and the distance between these topographic features: we have shown that the first parameter clearly controls the spectral response in the high frequency regime (Eq. (7)), generating amplification and reduction at convex and concave topographies

respectively. On the other hand, the second parameter controls the level of topographic interaction between singular elements, in such a way that at low frequencies topographic irregularities are perceived as very small and very close to each other, producing a response controlled by the isolated topography. These aspects of the response can be taken as points of departure to produce revised site coefficients taking into account the spatial variability of the response due to topographic effects. Particularly, in work-in-progress, we are exploring the concept of topographic interaction in order to relate the distance between topographic features and frequency content and thus study the feasibility of locally-based aggravation factors that can be applied to simple, local geometries depending upon the frequency range of interest. As suggested by results from diffraction theory, key to this problem is precisely the distance between sources of diffracted waves.

Acknowledgements

This project was conducted with financial support from "Departamento Administrativo de Ciencia, Tecnología e Innovación, COLCIENCIAS", Colombia and from Universidad EAFIT, Colombia through the 528-2012 Program for conducting Ph.D. Studies in Colombia. The authors would like to thank the objective and constructive comments made by three anonymous reviewers. These comments and suggestions were used to enhance the quality of the paper.

Appendix: Variation of the error parameter in the canonical topographies

(Fig. 22) (Fig. 23) (Fig. 24) (Fig. 25) (Fig. 26) (Fig. 27) (Fig. 28) (Fig. 29) (Fig. 30) (Fig. 31)

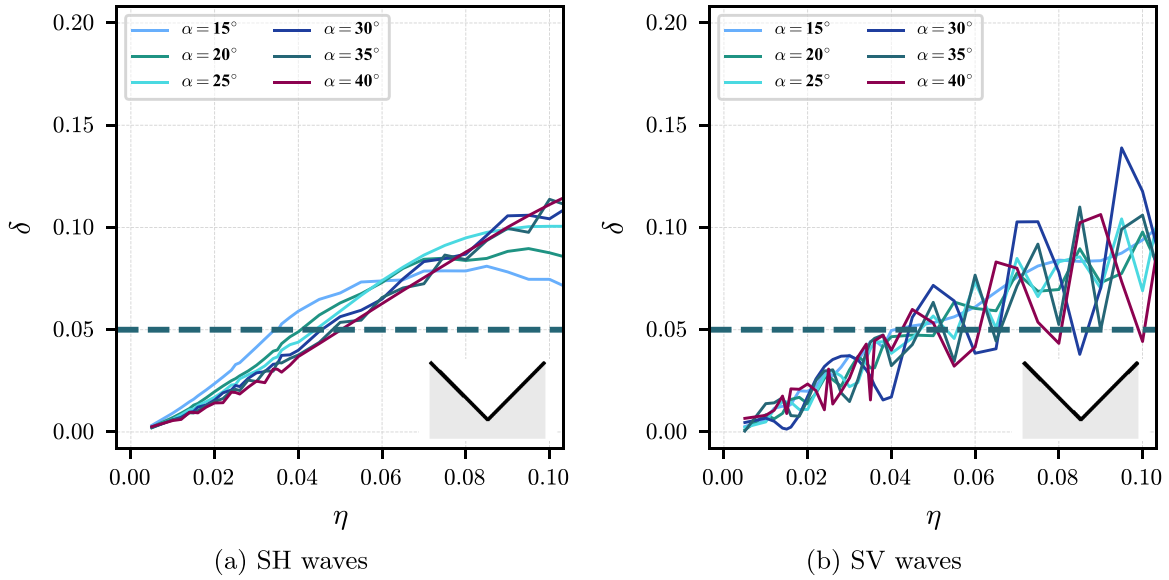

Fig. 22. Variation of the error measure δ vs dimensionless frequency η in a concave wedge subjected to incident *SH* and *SV* waves for slope angles in the range [15°, 40°] and distance parameter $d = 100$. The dashed horizontal line intercepting the plot at η_{max} corresponds to the limit value of $\delta = 0.05$.

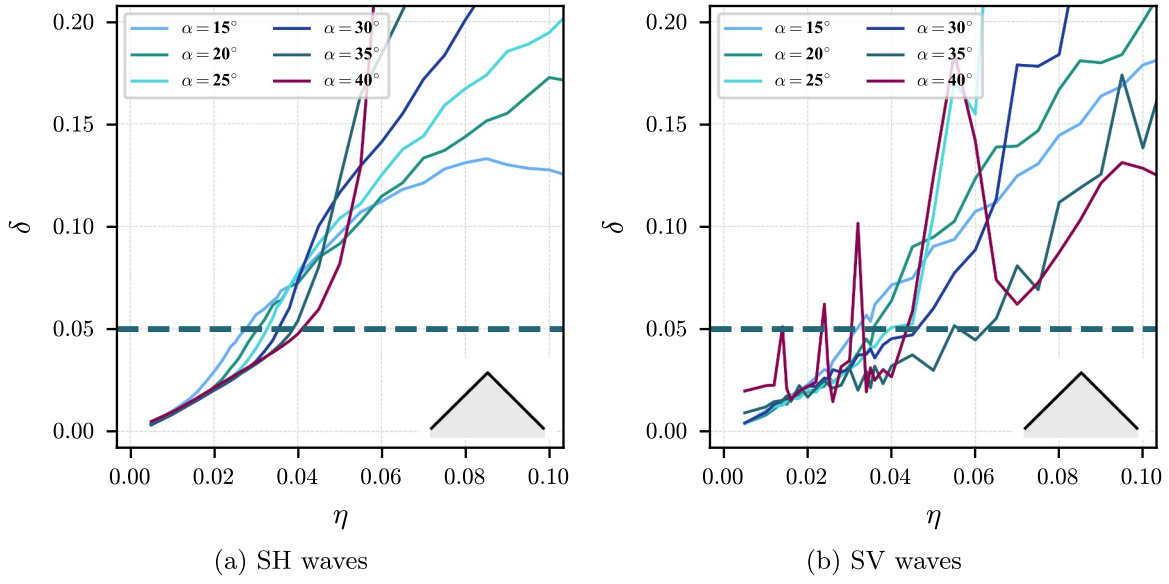

Fig. 23. Variation of the error measure δ vs dimensionless frequency η in a convex wedge subjected to incident *SH* and *SV* waves for slope angles in the range [15°, 40°] and distance parameter $d = 100$. The dashed horizontal line intercepting the plot at η_{max} corresponds to the limit value of $\delta = 0.05$.

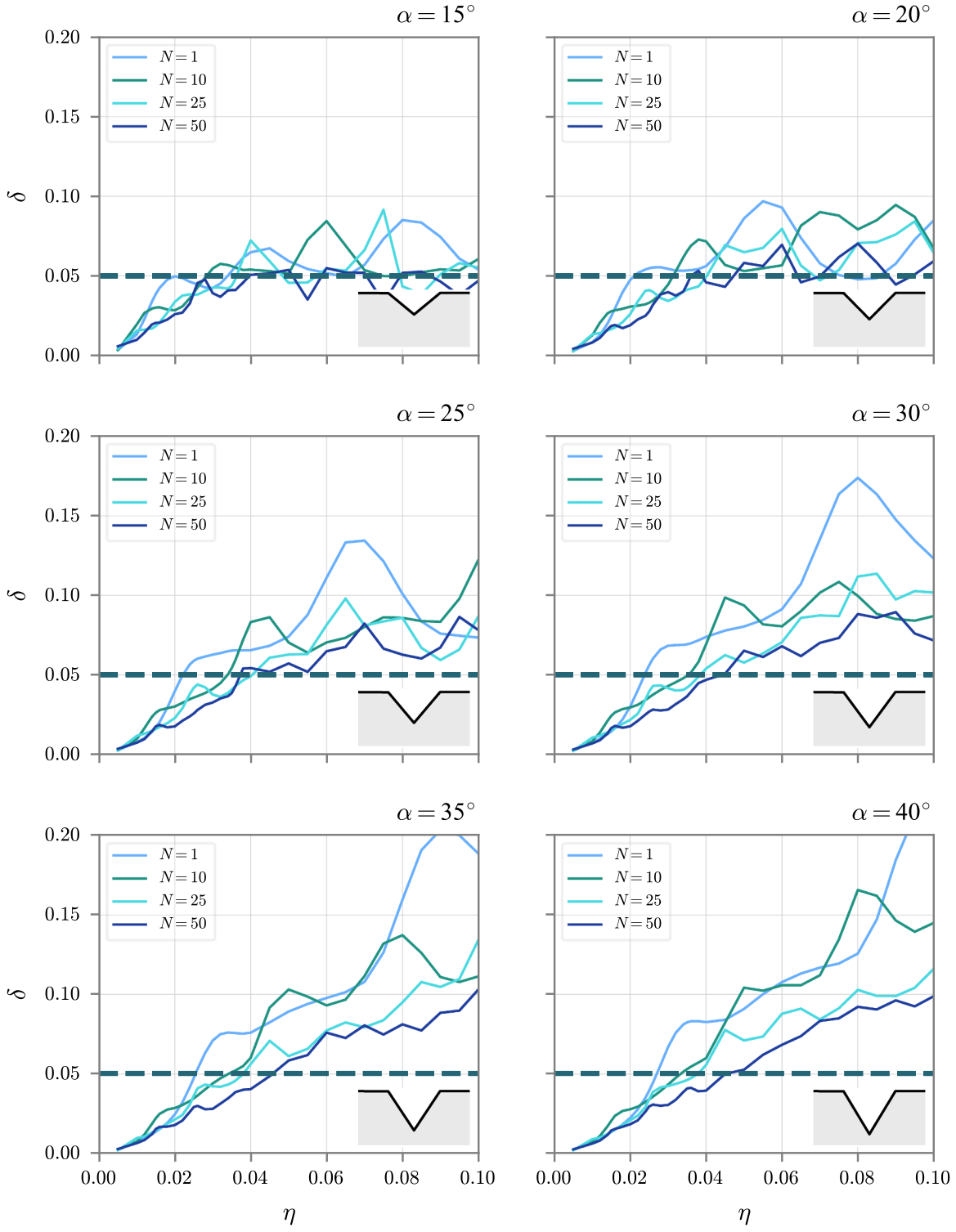

Fig. 24. Variation of the error parameter δ vs dimensionless frequency η in V-shaped canyons of slope angle α in the range [15°, 20°, 25°, 30°, 35°, 40°] and subjected to incident *SH* waves. Each plot corresponds to a different separation between topographic elements as indicated by the distance parameter L_W. The dashed horizontal line intercepting each plot at the maximum frequency η_{max} indicates the acceptable limiting value of $\delta = 0.05$.

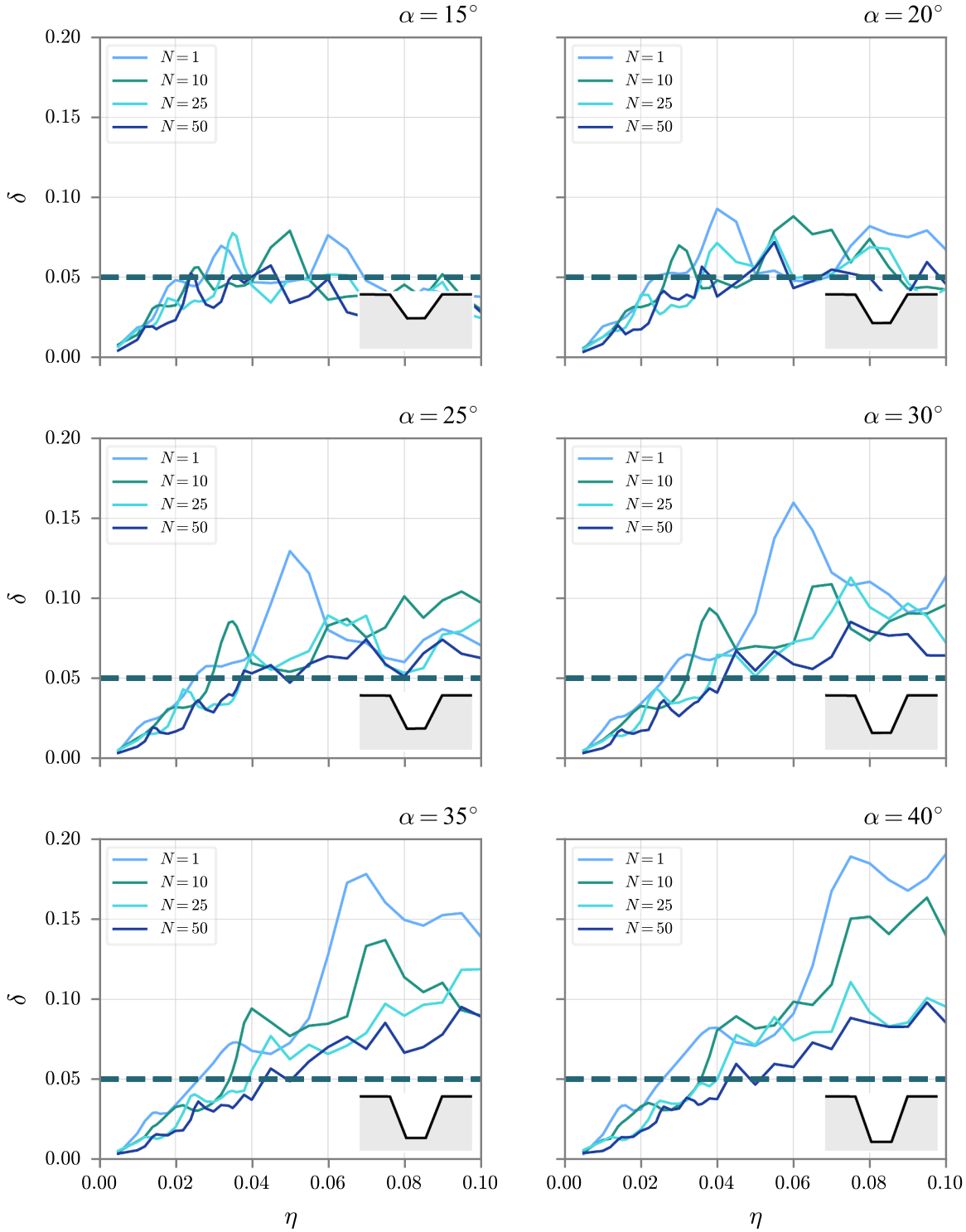

Fig. 25. Variation of the error parameter δ vs dimensionless frequency η in trapezoidal canyons of slope angle α in the range [15°, 20°, 25°, 30°, 35°, 40°] and subjected to incident *SH* waves. Each plot corresponds to a different separation between topographic elements as indicated by the distance parameter L_W. The dashed horizontal line intercepting each plot at the maximum frequency η_{max} indicates the acceptable limiting value of $\delta = 0.05$.

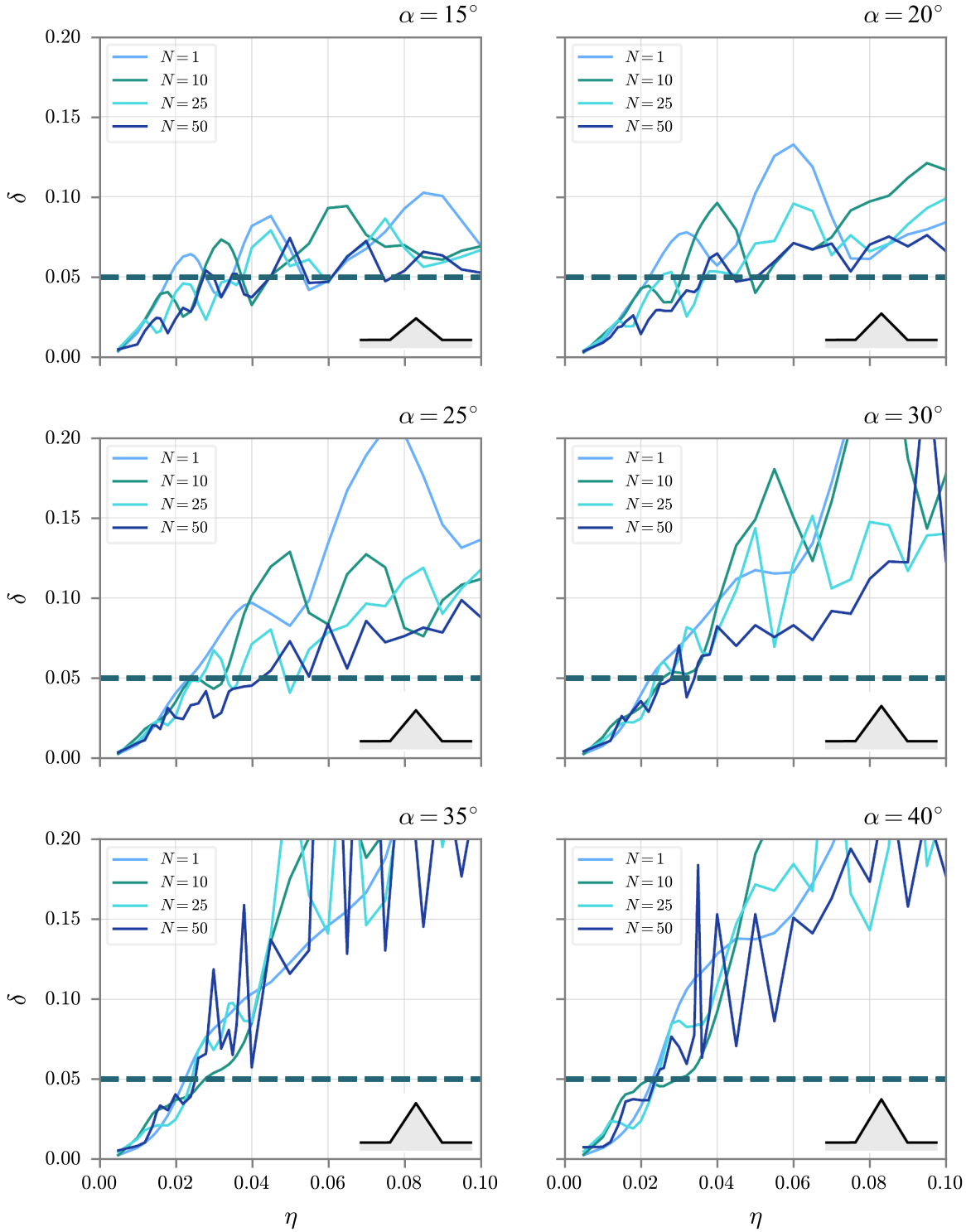

Fig. 26. Variation of the error parameter δ vs dimensionless frequency η in trapezoidal canyons of slope angle α in the range [15°, 20°, 25°, 30°, 35°, 40°] and subjected to incident *SH* waves. Each plot corresponds to a different separation between topographic elements as indicated by the distance parameter L_W. The dashed horizontal line intercepting each plot at the maximum frequency η_{max} indicates the acceptable limiting value of $\delta = 0.05$.

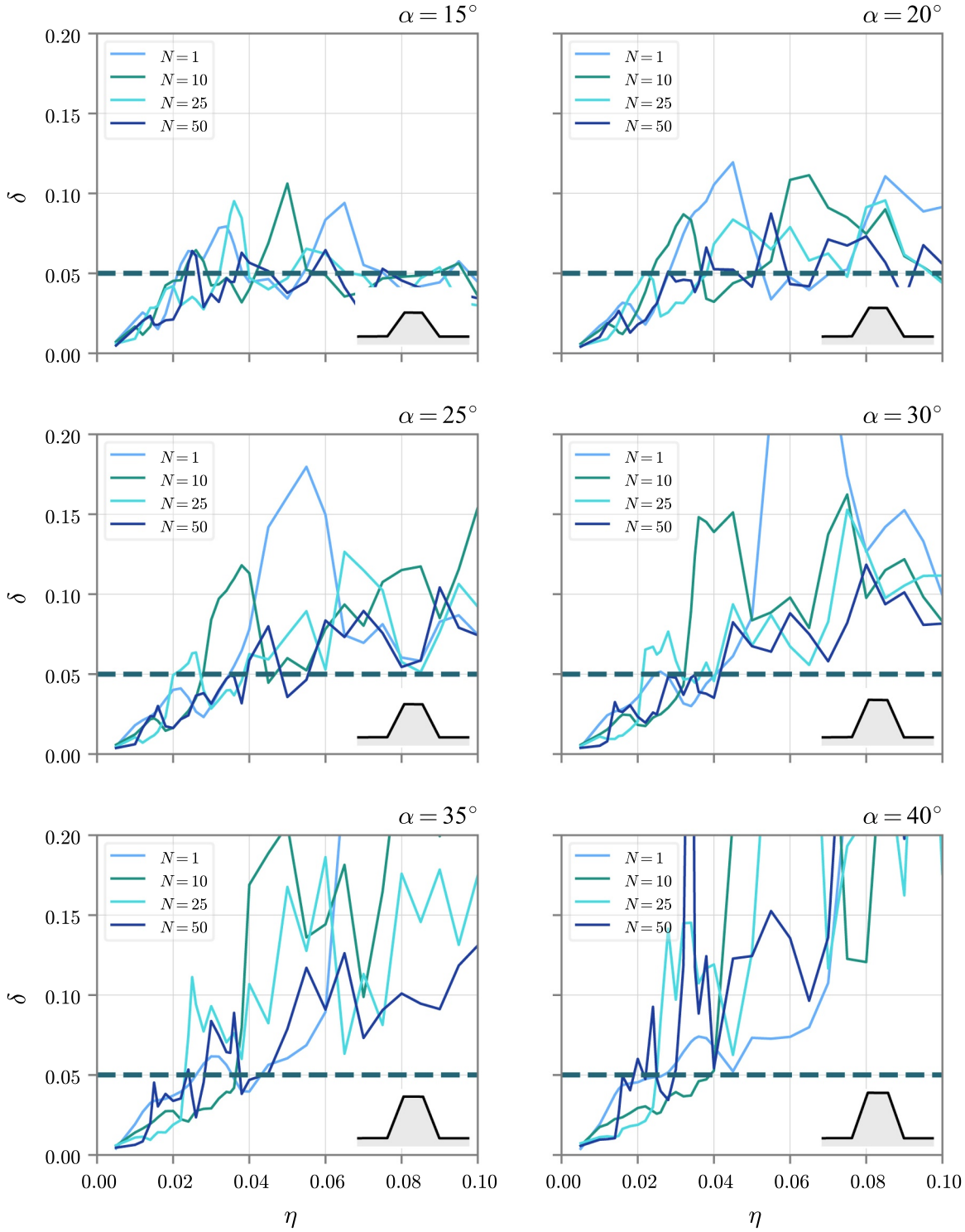

Fig. 27. Variation of the error parameter δ vs dimensionless frequency η in trapezoidal canyons of slope angle α in the range [15°, 20°, 25°, 30°, 35°, 40°] and subjected to incident *SH* waves. Each plot corresponds to a different separation between topographic elements as indicated by the distance parameter L_W. The dashed horizontal line intercepting each plot at the maximum frequency η_{max} indicates the acceptable limiting value of δ = 0.05.

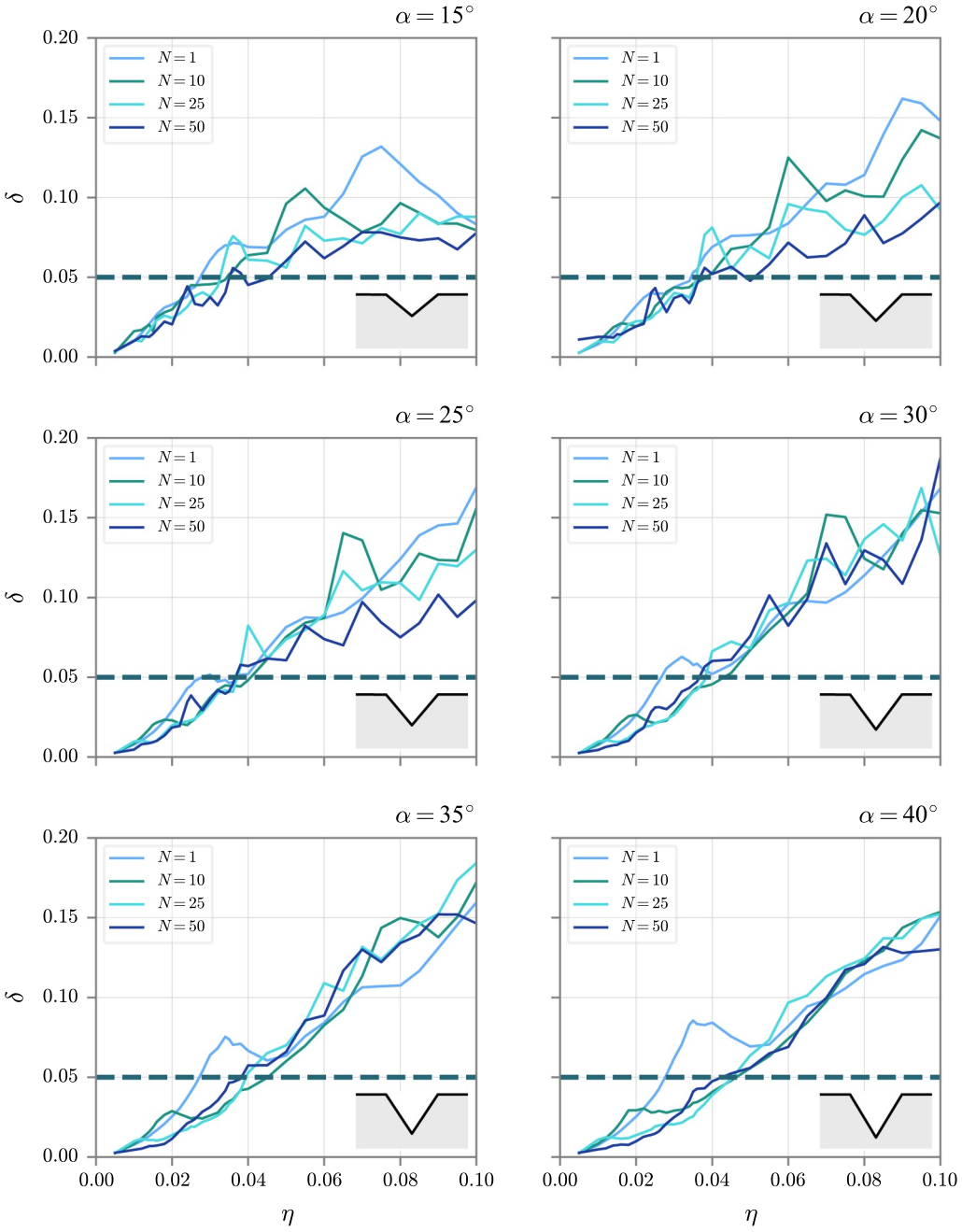

Fig. 28. Variation of the error parameter δ vs dimensionless frequency η in trapezoidal canyons of slope angle α in the range [15°, 20°, 25°, 30°, 35°, 40°] and subjected to incident *SH* waves. Each plot corresponds to a different separation between topographic elements as indicated by the distance parameter L_W. The dashed horizontal line intercepting each plot at the maximum frequency η_{max} indicates the acceptable limiting value of $\delta = 0.05$.

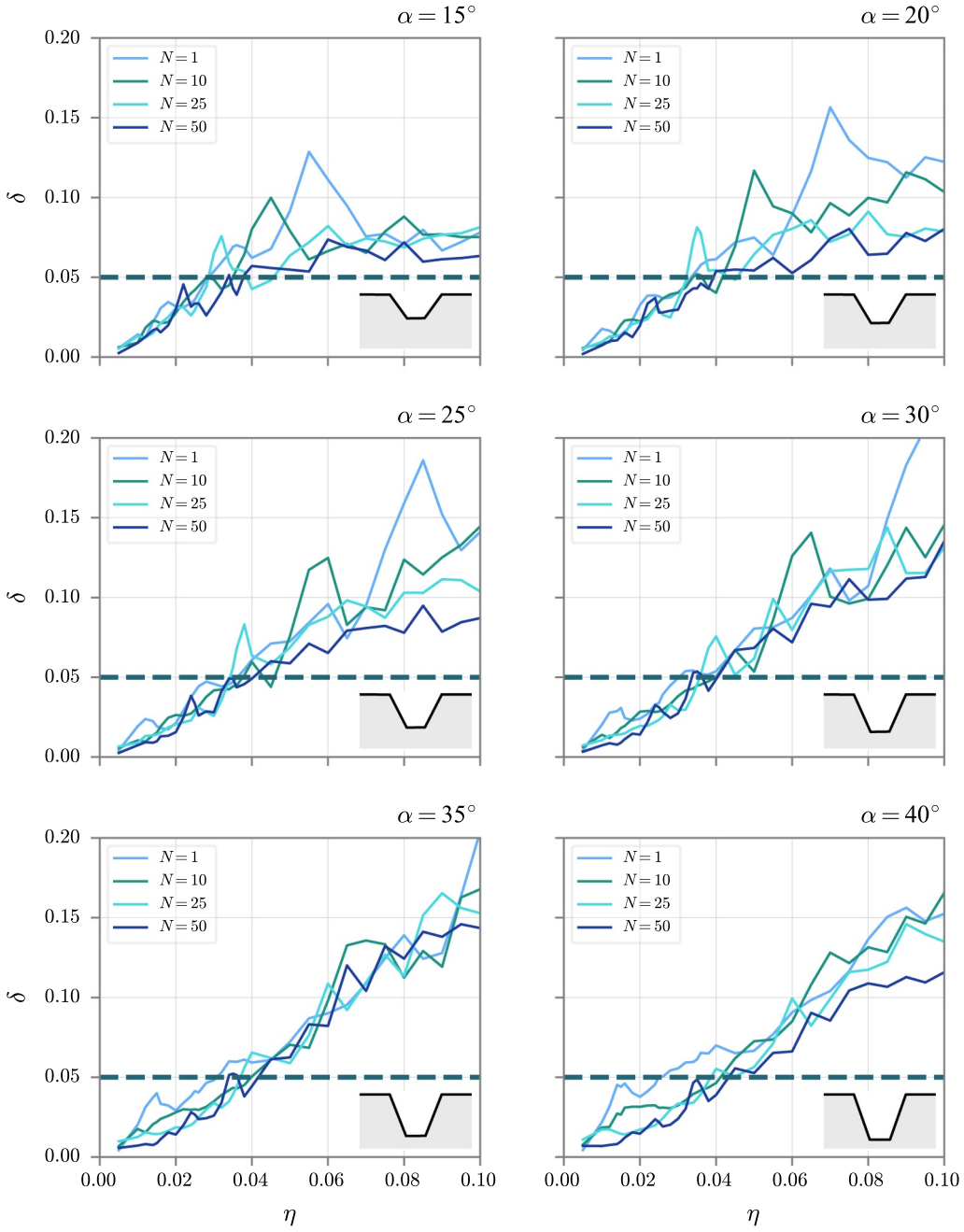

Fig. 29. Variation of the error parameter δ vs dimensionless frequency η in trapezoidal canyons of slope angle α in the range [15°, 20°, 25°, 30°, 35°, 40°] and subjected to incident *SH* waves. Each plot corresponds to a different separation between topographic elements as indicated by the distance parameter L_W. The dashed horizontal line intercepting each plot at the maximum frequency η_{max} indicates the acceptable limiting value of $\delta = 0.05$.

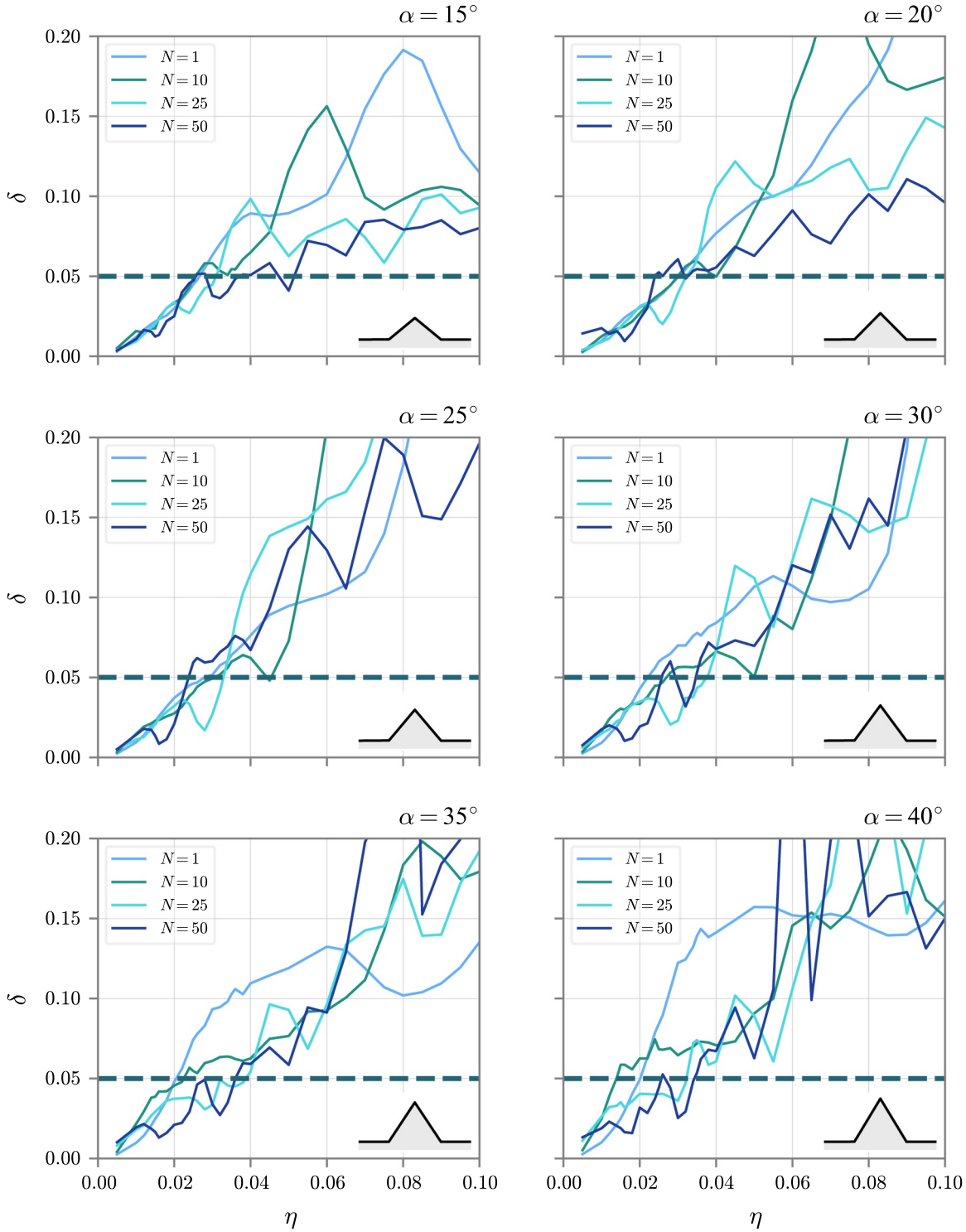

Fig. 30. Variation of the error parameter δ vs dimensionless frequency η in trapezoidal canyons of slope angle α in the range [15°, 20°, 25°, 30°, 35°, 40°] and subjected to incident *SH* waves. Each plot corresponds to a different separation between topographic elements as indicated by the distance parameter L_W. The dashed horizontal line intercepting each plot at the maximum frequency η_{max} indicates the acceptable limiting value of $\delta = 0.05$.

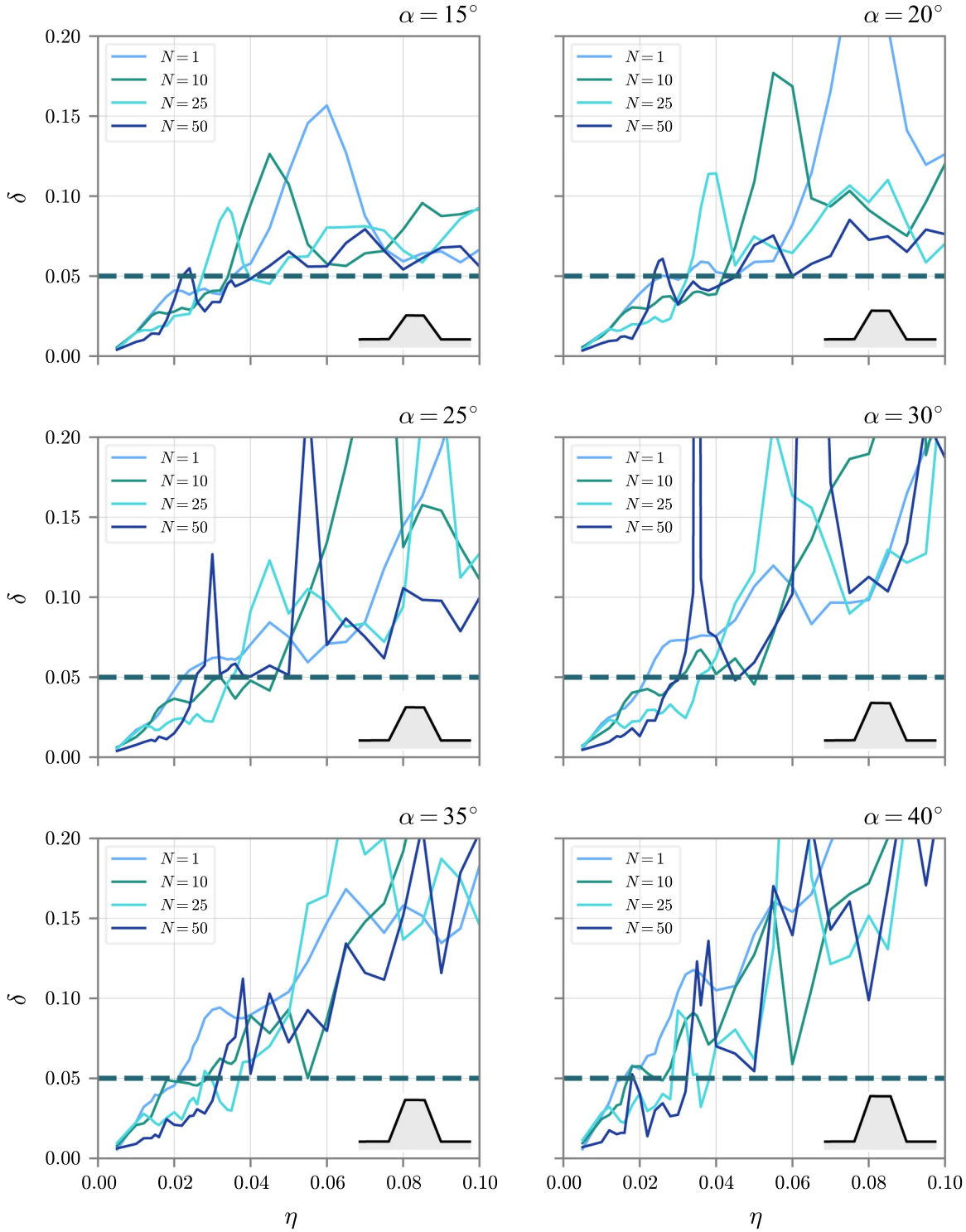

Fig. 31. Variation of the error parameter δ vs dimensionless frequency η in trapezoidal hills of slope angle α in the range [15°, 20°, 25°, 30°, 35°, 40°] and subjected to incident *SV* waves. Each plot corresponds to a different separation between topographic elements as indicated by the distance parameter L_W. The dashed horizontal line intercepting each plot at the maximum frequency η_{max} indicates the acceptable limiting value of δ = 0.05.

References

[1] AFPS French Association for Earthquake Engineering, French Seismic Code. Guidelines for Seismic Microzonation Studies 1995.

[2] Aki K, Larner K. Surface motion of a layered medium having an irregular interface due to incident plane SH waves. J Geophys Res 1970;75:5.

[3] Al Atik L, Abrahamson N. An improved method for nonstationary spectral matching. Earthq Spectra 2010;26(3):601–17.

[4] ASCE, 2010. Minimum design loads for buildings and other structures, p. Chapter 21.

[5] Ashford SA, Sitar N, Lysmer J, Deng N. Topographic effects on the seismic response of steep slopes. Bull Seismol Soc Am 1997;87(3):701–9.

[6] Asimaki D, Mohammadi K. On the complexity of seismic waves trapped in irregular topographies. Soil Dyn Earthq Eng 2018;114:424–37.

[7] Assimaki D, Jeong S. Ground-motion observations at hotel Montana during the M 7.0 2010 Haiti earthquake: topography or soil amplification? Bull Seismol Soc Am 2013;103(5):2577–90.

[8] Assimaki D, Gazetas G, Kausel E. Effects of local soil conditions on the topographic aggravation of seismic motion: parametric investigation and recorded field evidence from the 1999 Athens earthquake. Bull Seismol Soc Am 2005;95(3):1059–89.
[9] Banerjee PK, Butterfield R. Boundary element methods in engineering science. 17. London: McGraw-Hill; 1981.
[10] Bard P, Czitrom G, Durville J, Godefroy P, Meneroud J, Mouroux P, Pecker A. Guidelines for seismic microzonation studies, Delegation of major risks of the French Ministry of the environment-direction for prevention, pollution and risks 1995.
[11] Bathe K-J. Finite element procedures, Klaus-Jurgen Bathe 2006.
[12] Bielak J, Loukakis K, Hisada Y, Yoshimura C. Domain reduction method for 3D earthquake modelling in localized regions. Part I: theory. Bull Seismol Soc Am 2003;93(2):817–24.
[13] Borja RI, Chao H-Y, Montáns FJ, Lin C-H. Nonlinear ground response at Lotung LSST site. J Geotech Geoenviron Eng 1999;125(3):187–97.
[14] Bouchon M, Barker JS. Seismic response of a hill: the example of Tarzana, California. Bull Seismol Soc Am 1996;86(1):66–72.
[15] Chávez-García F, Raptakis D, Makra K, Pitilakis K. Site effects at Euroseistest–II. Results from 2D numerical modeling and comparison with observations. Soil Dyn Earthq Eng 2000;19(1):23–39.
[16] Geli L, Bard P-Y, Jullien B. The effect of topography on earthquake ground motion: a review and new results. Bull Seismol Soc Am 1988;78(1):42–63.
[17] Gomez J, Jaramillo J, Saenz M, Vergara J. A superposition based diffraction technique to study site effects in earthquake engineering. Int. J. Geophys. 2016.
[18] Han F, Wang GZ, Kang CY. Scattering of SH-waves on triangular hill joined by semicylindrical canyon. Appl Math Mech 2011;32(3):309–26.
[19] Hashash YM, Park D. Non-linear one-dimensional seismic ground motion propagation in the Mississippi embayment. Eng Geol 2001;62(1–3):185–206.
[20] Hughes TJ, The finite element method: linear static and dynamic finite element analysis, Courier Corporation 2012.
[21] Jaramillo JD, Gomez JD, Saenz M, Vergara JC. Analytic approximation to the scattering of antiplane shear waves by free surfaces of arbitrary shape via superposition of incident, reflected and diffracted rays. Geophys J Int 2012;192(3):1132–43.
[22] JRC European Commission, Eurocode, C., International Code Council, Eurocode 8: Seismic Design of Buildings Worked examples, vol. 1 2004.
[23] Keller JB. Geometrical theory of diffraction. J Opt Soc Am 1962;52(2):116–30.
[24] Komatitsch D, Liu Q, Tromp J, Süss P, Stidham C, Shaw JH. Simulations of strong ground motion in the Los Angeles basin based upon the spectral-element method. Bull Seismol Soc Am 2004;94(1):187–206.
[25] Kouyoumjian RG, Pathak PH. A uniform geometrical theory of diffraction for an edge in a perfectly conducting surface. Proc IEEE 1974;62(11):1448–61.
[26] Makra K, Chávez-García FJ. Site effects in 3d basins using 1d and 2d models: an evaluation of the differences based on simulations of the seismic response of euroseistest. Bull Earthq Eng 2016;14(4):1177–94.
[27] Makra K, Chávez-García FJ, Raptakis D, Pitilakis K. Parametric analysis of the seismic response of a 2D sedimentary valley: implications for code implementations of complex site effects. Soil Dyn Earthq Eng 2005;25(4):303–15.
[28] Massa M, Barani S, Lovati S. Overview of topographic effects based on experimental observations: meaning, causes and possible interpretations. Geophys J Int 2014;197(3):1537–50.
[29] Mohammadi K. Geometry and stratigraphy parameterization of topography effects: from the infinite wedge to 3D convex features [Ph.D. thesis]. Georgia Institute of Technology; 2015.
[30] Nguyen KV, Gatmiri B. Evaluation of seismic ground motion induced by topographic irregularity. Soil Dyn Earthq Eng 2007;27:183–8.
[31] Poursartip B, Fathi A, Kallivokas LF. Seismic wave amplification by topographic features: a parametric study. Soil Dyn Earthq Eng 2017;92(July (2016)):503–27.
[32] Restrepo D. Effects of soil nonlinearity on ground response in 3d simulations - an application to the salt lake city basin 2011.
[33] Restrepo D, Bielak J, Serrano R, Gómez J, Jaramillo J. Effects of realistic topography on the ground motion of the colombian andes-a case study at the aburrá valley, antioquia. Geophys J Int 2016;204(3):1801–16.
[34] Sánchez-Sesma FJ. Diffraction of elastic SH waves by wedges. Bull Seismol Soc Am 1985;75(5):1435–46.
[35] Sánchez-Sesma FJ. Elementary solutions for response of a wedge-shaped medium to incident SH and SV Waves. Bull Seismol Soc Am 1990;80(3):737–42.
[36] Sánchez-Sesma FJ, Rosenblueth E. Ground motion at canyons of arbitrary shape under incident SH waves. Earthq Eng Struct Dyn 1979;7(5):441–50.
[37] Shnabel P. Shake, a computer program for earthquake response analysis of horizontal layered sites, Report No. EERC 72-12 1972.
[38] Taborda R, Bielak J. Large-scale earthquake simulation: computational seismology and complex engineering systems. Comput Sci Eng 2011;13(4):14–27.
[39] Taborda R, Bielak J, Restrepo D. Earthquake ground-motion simulation including nonlinear soil effects under idealized conditions with application to two case studies. Seismol Res Lett 2012;83(6):1047–60.
[40] Trifunac MD. Scattering of plane SH waves by a semicylindrical canyon. Earthq Eng Struct Dyn 1973;1:267–81.
[41] Trifunac MD, Hudson DE. Analysis of the Pacoima dam accelerogram-San Fernando, California, earthquake of 1971. Bull Seismol Soc Am 1971;61(5):1393–411.
[42] Tsaur D-H, Chang K-H. An analytical approach for the scattering of SH waves by a symmetrical V-shaped canyon: shallow case. Geophys J Int 2008;174(1):255–64.
[43] Tsaur D-H, Chang K-H, Hsu M-S. An analytical approach for the scattering of SH waves by a symmetrical V-shaped canyon: deep case. Geophys J Int 2010;183(3):1501–11.
[44] Vucetic M. Normalized behavior of clay under irregular cyclic loading. Can Geotech J 1990;27(1):29–46.
[45] Yoshimura C, Bielak J, Hisada Y, Fernández A. Domain reduction method for three-dimensional earthquake modeling in localized regions, part II: verification and applications. Bull Seismol Soc Am 2003;93(2):825–40.
[46] Zhang N, Gao Y, Li D, Wu Y, Zhang F. Scattering of SH waves induced by a symmetrical V-shaped canyon: a unified analytical solution. Earthq Eng Eng Vib 2012;11(4):445–60.